The Meteoritical Society

Meteoritics & Planetary Science 52, Nr 2, 372–390 (2017)
doi: 10.1111/maps.12797

NWA 10214—An LL3 chondrite breccia with an assortment of metamorphosed, shocked, and unique chondrite clasts

Alan E. RUBIN[1,2*], John P. BREEN[3], Junko ISA[1], and Sean TUTOROW[4]

[1]Department of Earth, Planetary, and Space Sciences, University of California, Los Angeles, California 90095–1567, USA
[2]Institute of Geophysics and Planetary Physics, University of California, Los Angeles, California 90095–1567, USA
[3]Department of Chemistry and Biochemistry, University of California, Los Angeles, California 90095–1567, USA
[4]eegooblago meteorites, Greeley, Colorado 80634, USA
[*]Corresponding author. E-mail: aerubin@ucla.edu

(Received 13 November 2015; revision accepted 20 October 2016)

Abstract–NWA 10214 is an LL3-6 breccia containing ~8 vol% clasts including LL5, LL6, and shocked-darkened LL fragments as well as matrix-rich Clast 6 (a new kind of chondrite). This clast is a dark-colored, subrounded, 6.1 × 7.0 mm inclusion, consisting of 60 vol% fine-grained matrix, 32 vol% coarse silicate grains, and 8 vol% coarse opaque grains. The large chondrules and chondrule fragments are mainly Type IB; one small chondrule is Type IIA. Also present are one 450 × 600 μm spinel-pyroxene-olivine CAI and one 85 × 110 μm AOI. Clast 6 possesses a unique set of properties. (1) It resembles carbonaceous chondrites in having relatively abundant matrix, CAIs, and AOIs; the clast's matrix composition is close to that in CV3 Vigarano. (2) It resembles type-3 OC in its olivine and low-Ca pyroxene compositional distributions, and in the Fe/Mn ratio of ferroan olivine grains. Its mean chondrule size is within 1σ of that of H chondrites. The O-isotopic compositions of the chondrules are in the ordinary- and R-chondrite ranges. (3) It resembles type-3 enstatite chondrites in the minor element concentrations in low-Ca pyroxene grains and in having a high low-Ca pyroxene/olivine ratio in chondrules. Clast 6 is a new variety of type-3 OC, somewhat more reduced than H chondrites or chondritic clasts in the Netschaevo IIE iron; the clast formed in a nebular region where aerodynamic radial drift processes deposited a high abundance of matrix material and CAIs. A chunk of this chondrite was ejected from its parent asteroid and later impacted the LL body at low relative velocity.

INTRODUCTION

There is a large diversity of dark-colored clasts in ordinary chondrites (OC). Some clasts are fragments of objects that formed in the solar nebula before being chemically and physically altered on their parent asteroids. This set includes CM chondrite clasts (Fodor et al. 1976; Fodor and Keil 1978; Keil and Fodor 1980; Nozette and Wilkening 1982; Lipschutz et al. 1989; Rubin and Bottke 2009) (which also occur in HED achondrites; Zolensky et al. 1996), CI-like clasts (Leitch and Grossman 1977; Zolensky et al. 2003, 2015), matrix-rich lumps (Kurat 1970; Leitch and Grossman 1977; Scott et al. 1984), microchondrule-bearing clasts (Fodor et al. 1977; Rubin 1982, 1989), matrix-rich clasts (e.g., Dobrică and Brearley 2014), and carbon-rich aggregates (Scott et al. 1981, 1988; Brearley 1990; Rubin et al. 2005). Other dark clasts are shock-modified ordinary-chondrite materials; these include shock-darkened chondritic fragments (Fodor and Keil 1978; Williams et al. 1985) and some impact-melt-rock clasts (Leitch and Grossman 1977; Rubin et al. 1983).

Most clasts within OC regolith breccias were derived from projectiles. Some of these clasts were partly impact melted when they collided with their target (Rubin et al. 1983; Rubin and Bottke 2009); some may also have been aqueously altered, either on their original parent body or on their target asteroid (Rubin et al. 2005).

Dark clasts within type-3 OC were derived from several sources. Some probably agglomerated along with chondrules at the earliest stages of accretion (e.g., matrix lumps and microchondrule-bearing clasts; Scott et al. 1984; Rubin 1989), others may have formed by collisions on the parent body (e.g., melt-rock clasts in some L3 and LL3 chondrites; Semenenko and Perron 2005; Semenenko et al. 2005; Johnson et al. 2015), and a few may be fragments of projectiles (e.g., a black inclusion in LL3 Krymka; Grossman et al. 1980).

We report here a dark-colored chondritic clast that represents a new kind of chondrite that was incorporated into NWA 10214 as a projectile fragment. It possesses a unique set of properties, individually characteristic of different chondrite varieties.

ANALYTICAL PROCEDURES

Thin section UCLA 2319 of NWA 10214 was examined microscopically in transmitted and reflected light and by backscattered electron (BSE) imaging. BSE images were made at UCLA with two instruments (1) the JEOL JXA-8200 electron microprobe using an acceleration voltage of 15 keV and a working distance of ~11 mm and (2) the TESCAN VEGA 3 scanning electron microscope (SEM) using a 20 keV acceleration voltage and a working distance of ~17 mm. The modal abundance of matrix in the dark clast was determined from BSE images using Adobe Photoshop software. Modal abundances of mineral components in the clast were made with a Swift automated point counter.

Mineral compositions were determined with the JEOL microprobe, using a focused beam, natural and synthetic standards, an acceleration voltage of 15 keV, a 15 nA sample current, 20 s counting times per element, and ZAF corrections. The Co values of metal and sulfide grains were corrected for the interference of the Fe-K_β peak with the Co-K_α peak. The composition of the fine-grained matrix in Clast 6 was determined with the JEOL probe under the same conditions but with a 3 μm diameter beam.

Oxygen-isotope measurements of chondrules and the CAI (Ca-Al-rich inclusion) in Clast 6 were obtained in situ with the UCLA Cameca ims 1270 ion microprobe using a primary Cs^+ beam and negative secondary ions. Samples were sputtered with a primary beam intensity of 10 kV acceleration voltage focused to about a 20 μm spot size with a primary beam of about 2 nA. A normal incident electron gun was used to compensate for possible sample charging. Oxygen isotopes were simultaneously measured on a multicollector. Two Faraday cups and one electron multiplier were employed in the analysis. A mass resolving power >5000 was used to resolve the interference of ^{16}OH at mass 17. San Carlos olivine ($\delta^{18}O$ = 5.2‰; Young et al. 2014) was used for the oxygen-isotope standard. With these conditions, the 2 σ reproducibility of San Carlos olivine measurements (n = 5) for $\delta^{18}O$ and $\delta\ ^{17}O$ were 0.53‰ and 0.71‰, respectively. Oxygen-isotopic compositions are given in units of per mil (‰) relative to SMOW (standard mean ocean water) and expressed as $\Delta^{17}O$, defined as the deviation from the terrestrial fractionation (TF) line on the standard three-isotope graph, where:

$$\Delta^{17}O = \delta^{17}O - 0.52 \times \delta^{18}O,$$

$$\delta^{17}O = [((^{17}O/^{16}O)_{sample}/(^{17}O/^{16}O)_{SMOW}) - 1] \times 1000,$$

$$\delta^{18}O = [((^{18}O/^{16}O)_{sample}/(^{18}O/^{16}O)_{SMOW}) - 1] \times 1000.$$

RESULTS

Petrography, Mineralogy, and Classification of the NWA 10214 Whole Rock

NWA 10214 was found in Morocco as a single 1816 g stone. The host (Fig. 1) contains sharply defined chondrules of all major textural varieties: porphyritic olivine (PO), porphyritic pyroxene (PP), porphyritic olivine-pyroxene (POP), porphyritic pyroxene-olivine (PPO), barred olivine (BO), radial pyroxene (RP), cryptocrystalline (C), and granular olivine-pyroxene (GOP). The chondrules range in apparent diameter from ~150 to 6500 μm and average ~500 μm. We also identified a 530 × 630 μm sized ellipsoidal "dark-zoned chondrule" (cf. Dodd and Van Schmus 1971) very similar in appearance to an object in LL3 Semarkona described by Rubin (1984). Dark-zoned chondrules are concentrically zoned; their outer mantles contain small grains of troilite. These objects were later dubbed agglomeratic olivine (AO) chondrules by Weisberg and Prinz (1994, 1996). In addition to intact chondrules, the NWA 10214 host contains numerous chondrule fragments and isolated mineral grains.

Some of the opaque phases in the rock occur in 200–300 μm sized globular assemblages that consist of moderately fine-grained intergrowths of metallic Fe-Ni (kamacite and taenite) with 4–25 μm sized irregular patches of troilite. Other 100–300 μm metallic Fe-Ni grains appear sulfide free. Also present are troilite nodules, 40–2550 μm in maximum dimension (Fig. 2), that contain no metallic Fe-Ni. The troilite is essentially pure FeS (Table 1). We found one small weathered grain of pentlandite with ~19 wt% Ni and ~0.80 wt% Co that had an analytical total of 94.1 wt%. No coarse grains of chromite are present.

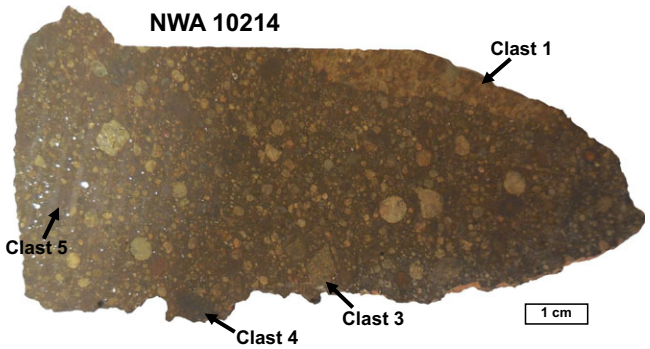

Fig. 1. Slab of the NWA 10214 LL3 chondrite breccia. The meteorite contains numerous well-defined chondrules and chondrule fragments and ~8 vol% clasts. Four of the described clasts are visible on this side of the slab including metamorphosed LL chondrites (Clasts 1 and 3) and shock-darkened LL chondrites (Clasts 4 and 5). Clast 5 is small and difficult to distinguish in the image. Clast 2 occurs on the opposite side of the slab and is not shown. (Color figure can be viewed at wileyonlinelibrary.com.)

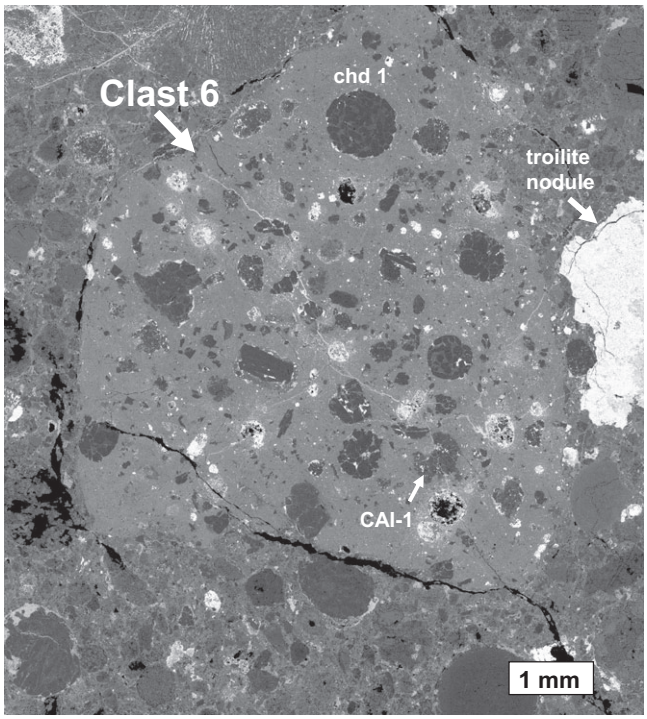

Fig. 2. Clast 6 is a subrounded object representing a new kind of chondritic material that shares characteristics with disparate chondrite groups. It contains 60 vol% matrix (light gray) in which are embedded pyroxene-rich chondrules, chondrule fragments, a moderate-size CAI, and an AOI. A large troilite nodule in the host is visible adjacent to Clast 6. BSE image.

The meteorite has been significantly weathered. Most of the silicate grains have been stained brown from mobilized oxidized iron. About 70% of the metallic Fe-Ni grains have been altered to limonite; this corresponds to weathering-stage W3 (Wlotzka 1993).

It is clear that NWA 10214 is an LL chondrite. The average chondrule size (~500 μm) is closest to that of mean LL chondrites (550 μm; table 7 of Friedrich et al. 2015). The mean olivine composition (Fa 28.1 ± 1.8; PMD = 5.1; n = 16) and mean kamacite Co content (1.5 ± 0.9 wt%; n = 7) are well within the equilibrated LL chondrite ranges (Fa 26.6–32.4; 1.42–37.0 wt% Co; Rubin 1990). Low-Ca pyroxene (Fs 15.9 ± 8.8, PMD = 48; n = 17) is unequilibrated and cannot be used as a classificatory parameter. Ca pyroxene is also present (Fs7.4–12.5 Wo14.2–38.0). From examination of the slabs and thin section of NWA 10214, we estimate that the meteorite contains ~2–3 vol% metallic Fe-Ni, corresponding to ~4–6 wt%. This is within the LL chondrite range (3.0–6.0 wt%; table 4 of Gomes and Keil 1980). (The PMD value [percent mean deviation] is calculated from the mean absolute-value deviation of the FeO concentration of individual measurements [in wt%] from the mean of those measurements, divided by the mean FeO concentration, and multiplied by 100%; Dodd et al. 1967.)

The Meteoritical Bulletin Database classifies NWA 10214 as an LL3 chondrite. The petrologic subtype of the host can be roughly estimated from the classificatory data listed in table 1 of Huss et al. (2006). The sharply defined chondrules and absence of coarse chromite and plagioclase grains in NWA 10214 indicate that the host is indeed petrologic type 3. The absence of clear, transparent isotropic glassy mesostases in the chondrules is characteristic of subtype 3.6–3.9. Most of the low-Ca pyroxene phenocrysts in chondrules exhibit polysynthetic twinning, indicative of subtype ≤3.9. The phenocrysts exhibit some patchy Fe-Mg zoning. Because the meteorite contains LL5 and LL6 clasts (see below), the whole rock should be classified as an LL3-6 breccia; the overall mineral compositional heterogeneity of the rock thus cannot accurately reflect the petrologic subtype of the type-3 host. The petrographic criteria, by themselves, indicate that the host is subtype 3.6–3.9.

The meteorite has been very weakly shocked. Most of the coarse olivine grains (isolated grains and chondrule phenocrysts) exhibit undulose extinction, contain irregular fractures, and lack planar fractures. This corresponds to a whole-rock shock stage of S2 (Stöffler et al. 1991).

The NWA 10214 whole rock is a breccia broadly similar to Ngawi (Scott and Taylor 1982) and NWA 7789 (Meteoritical Bulletin Database). Several different types of clasts are present in NWA 10214 (Fig. 1); the modal abundance of these clasts is ~8 vol%. With the exception of Clast 6 (described below), all of the clasts were examined only in an unpolished slab.

Table 1. Opaque phases in the NWA 10214 host and Clast 6.

	NWA 10214 host			Clast 6	
	Kamacite	Taenite	Troilite	Kamacite	Troilite
No. of analyses	7	1	4	3	5
Fe	90.9 ± 1.5	66.1	63.5 ± 0.5	91.3 ± 1.4	63.2 ± 0.4
Ni	6.8 ± 1.1	33.7	<0.03	4.9 ± 1.0	0.03 ± 0.02
Co	1.5 ± 0.9	1.4	<0.03	2.6 ± 2.4	<0.03
S	<0.03	<0.03	35.1 ± 0.2	<0.03	35.2 ± 0.2
Cr	<0.03	<0.03	<0.03	<0.03	0.03 ± 0.02
P	<0.03	<0.03	<0.03	<0.03	<0.03
total	99.2	101.2	98.6	98.8	98.5

Metamorphosed LL Chondrite Clasts

The largest clast, Clast 1, is light colored and has a chondritic texture (Fig. 1). It is ≥4 cm × ≥0.6 cm and occurs at one edge of the UCLA slab. Chondrules in Clast 1 average ~700 μm in apparent diameter; many exceed 1000 μm. Although the chondrules are readily delineated, all of them appear recrystallized; small chondrules are difficult to discern. No fine-grained silicate matrix material is evident. Metal grains range from ~50 to 650 μm; the modal abundance of metallic Fe-Ni is ~2 vol%. Also present in the clast is a 2.2 × 3.5 mm irregularly shaped troilite nodule that encloses several chondrules. The clast appears to be an LL5 chondrite.

Clast 2 is quasi-rectangular in shape, light in color, and 0.6 × 1.35 cm in size. It occurs on the opposite side of the slab in Fig. 1. There are a few very recrystallized 1–2 mm sized chondrules that are difficult to discern in the slab. Metal grains range from ~10 to 600 μm; the modal abundance of metallic Fe-Ni is ~3–4 vol%. The clast appears to be an LL6 chondrite.

Clast 3 is shaped like an ice-cream cone and is 4.5 × 7 mm in size (Fig. 1). The average size of the recrystallized chondrules within the clast is ~500 μm. The modal abundance of metallic Fe-Ni is very low, ~1 vol%. The clast is probably an LL5 or LL6 chondrite.

Shock Darkened LL Chondrite Clasts

Clast 4 is a 4.5 × 12 mm sized dark chondritic clast that also occurs at one edge of the UCLA slab (Fig. 1). Chondrules range in size from 180–1100 μm and average ~400–500 μm. The coarser metallic Fe-Ni grains range in size from 20 to 400 μm; the modal abundance of metal is ~3–5 vol%. Some 20 μm sized troilite grains are also present. A centimeter-long shock vein runs through the center of the clast from edge to edge; it transects and shears several chondrules. The dark interchondrule material contains numerous 1–6 μm sized metal and sulfide grains that are responsible for the silicate darkening evident in the clast (cf. Rubin 1992). The clast appears to be a shock-darkened LL chondrite analogous to shock-darkened clasts in some ordinary chondrite regolith breccias (e.g., Williams et al. 1985).

Clast 5 is 3 × 7 mm in size and quasi-elliptical in shape (Fig. 1). It contains ~90 vol% dark red chondrules, 200–1000 μm in size, surrounded by very dark fine-grained material. Metallic Fe-Ni is very fine grained. This clast also appears to be a shock-darkened, equilibrated LL chondrite. The red color of the chondrules is probably a result of terrestrial weathering. There are several smaller similar clasts located throughout the meteorite.

Clast 6—A Unique Chondrite

Petrography

Clast 6 is a subrounded object, 6.1 × 7.0 mm in size in the plane of the section; its surface area in the thin section is 26.6 mm^2 (Fig. 2). The clast appears dark colored on a cut surface of the whole rock and is very dark in thin section when viewed microscopically in transmitted light. Adobe Photoshop software applied to a BSE image of the clast coupled with modal analysis indicates that Clast 6 consists of 60 vol% fine-grained matrix material, 32 vol% coarse silicate grains (chondrules, chondrule fragments, a single CAI, a single AOI, and isolated 5–450 μm sized mafic mineral grains), and 8 vol% coarse opaque grains (including limonite). (AOI stands for amoeboid olivine inclusion, a.k.a. amoeboid olivine aggregate or AOA.) About 40% of the coarse silicate grains occur in chondrule fragments or as isolated grains rather than within largely intact chondrules.

The matrix consists predominantly of micrometer-to-submicrometer-sized silicate grains and minor ~0.3 μm sized troilite grains (Fig. 3). About 5 vol% of the matrix consists of coarser silicate grains most likely derived from broken chondrules. The clast-matrix boundary appears sharp (Fig. 3).

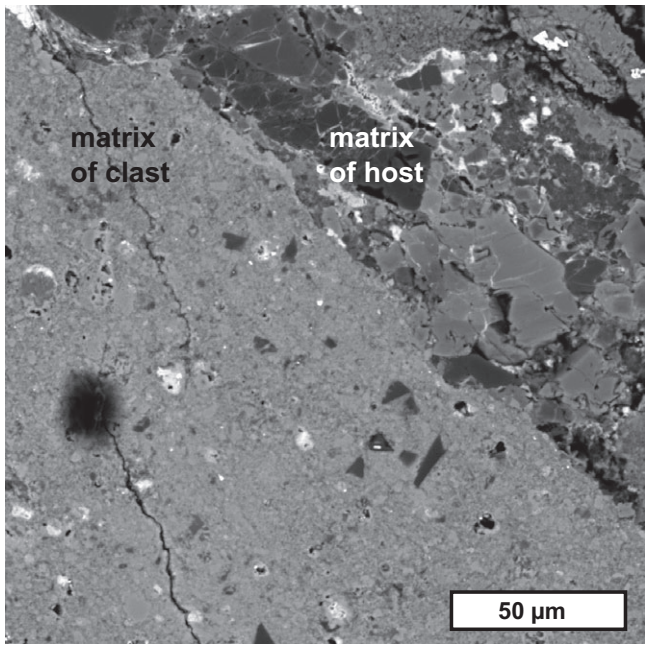

Fig. 3. Portion of the sharp clast-matrix boundary. The matrix of the clast (left) is composed mainly of micrometer-to-submicrometer-sized silicate grains, some coarser silicate grains derived from broken chondrules, and few opaque assemblages. The matrix of the LL chondrite host (right) is much coarser grained; it also contains chondrule fragments. BSE image.

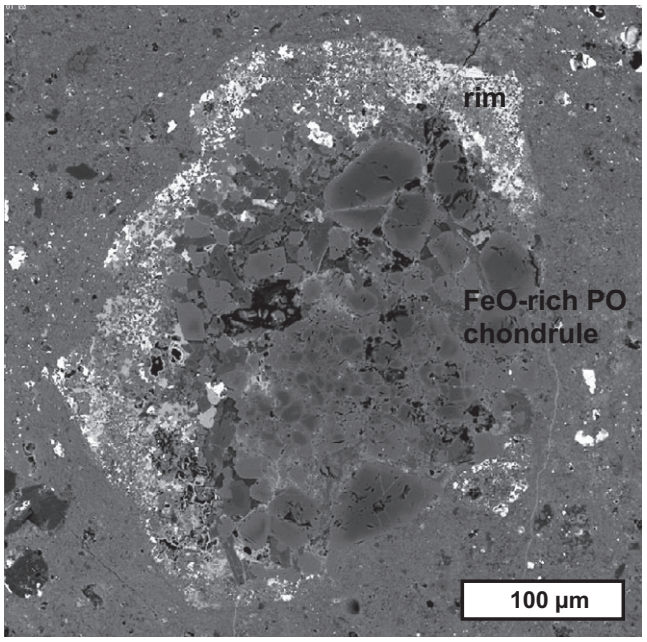

Fig. 4. Rare FeO-rich (Type IIA) PO chondrule containing a diversity of grain sizes. The thin rims around the individual olivine grains are more ferroan than the grain cores. About 60% of the chondrule is surrounded by a 10–45 μm thick, fine-grained opaque-rich rim. BSE image.

Table 2. Modal abundances of constituent phases in Clast 6.

	Points	vol%	wt%
Silicate	786	92.0	89.2
Metallic Fe-Ni	1	0.1	0.3
Troilite	38	4.4	6.2
Limonite	29	3.4	4.3
Total	854	99.9	100.0

The wt% values were calculated from vol% using the following densities (g cm^{-3}): silicate—3.25, metallic Fe-Ni—7.8, troilite—4.65, limonite—4.28.

The modal abundances of the different phases in the clast were determined by automated point-counting techniques (Table 2): 89.2 wt% silicate, 0.3 wt% metallic Fe-Ni (including kamacite and rare Ni-rich taenite), 6.2 wt% troilite, and 4.3 wt% limonite. A separate point count (n = 153) shows that 80% of the coarse mafic silicate grains are low-Ca pyroxene and 20% are olivine.

The apparent diameters of largely intact chondrules range from 100 to 810 μm with a mean of 330 ± 160 μm (n = 28). Most chondrules, chondrule fragments, and isolated mineral grains are composed mainly of low-Ca pyroxene; the low-Ca pyroxene/olivine ratio is 4:1. Among the 28 largely intact chondrules, 24 are PP or PPO (mostly PP); three are POP, and one chondrule (210 × 320 μm) is FeO-rich (i.e., Type IIA) PO (Fig. 4). There are no BO, RP, GOP, or C chondrules. All but one of the largely intact chondrules are low-FeO types (i.e., Type I); some isolated olivine grains contain significant amounts of FeO (13.3 ± 3.4 wt%; Table 3) and were presumably derived from broken FeO-rich (Type IIA) PO chondrules such the one in Fig. 4. This particular chondrule is partially surrounded by a 10–45 μm thick, fine-grained opaque-rich rim. Besides this chondrule, fine-grained rims around chondrules are rare to absent.

One chondrule fragment (Fig. 5), consisting mainly of elongated low-FeO low-Ca pyroxene grains, is surrounded by an igneous rim. The rim is composed predominantly of 5–10 μm sized low-Ca pyroxene and olivine grains. Many of the pyroxene grains are elongated; the one with the highest aspect ratio is 2 × 24 μm in size. Olivine grains in the rim are much more equant than the pyroxene grains. Besides this chondrule fragment, igneous rims are rare to absent.

About 80% of the mafic silicates in Chondrule 1 (the largest chondrule, 800 × 820 μm; Fig. 6) are elongated, polysynthetically twinned grains of low-Ca pyroxene (50–60 × 150–200 μm); about 20% of the silicates in the chondrule are ~70 μm sized olivine grains that are poikilitically enclosed within low-Ca pyroxene

Table 3. Mean compositions (wt%) of silicate phases in chondritic Clast 6.

	Chd 1 pyx	Chd 1 ol	Chd 2 pyx	Chd 3 pyx	Chd 4 pyx	High-Ca pyx	Isolated pyx	Isolated ol	Most ferroan isolated ol
No. of analyses	4	1	3	3	3	12	1	5	1
SiO_2	58.2 ± 0.4	41.0	58.1 ± 0.1	57.3 ± 0.6	57.9 ± 0.1	51.2 ± 1.5	53.9	40.1 ± 0.6	37.7
TiO_2	0.05 ± 0.01	0.04	0.04 ± 0.01	0.03 ± 0.01	0.05 ± 0.03	0.81 ± 0.5	0.11	<0.03	0.03
Al_2O_3	0.29 ± 0.06	<0.03	0.16 ± 0.02	0.19 ± 0.06	0.29 ± 0.08	5.5 ± 2.3	1.7	<0.03	<0.03
Cr_2O_3	0.47 ± 0.06	0.03	0.44 ± 0.02	0.62 ± 0.17	0.53 ± 0.06	2.3 ± 0.4	0.92	0.07 ± 0.07	<0.03
FeO	1.6 ± 0.1	4.4	2.0 ± 0.1	5.0 ± 0.6	1.7 ± 0.0	1.6 ± 0.2	14.1	13.3 ± 3.4	28.4
MnO	0.22 ± 0.04	0.27	0.20 ± 0.01	0.38 ± 0.11	0.21 ± 0.04	1.3 ± 0.2	0.51	0.34 ± 0.04	0.37
MgO	38.7 ± 0.1	54.2	38.6 ± 0.1	36.3 ± 0.6	38.6 ± 0.3	18.2 ± 1.7	27.5	47.8 ± 2.7	34.5
CaO	0.19 ± 0.04	0.04	0.16 ± 0.04	0.20 ± 0.07	0.18 ± 0.04	18.4 ± 1.5	1.8	0.09 ± 0.02	0.06
Na_2O	<0.03	<0.03	<0.03	0.04 ± 0.05	<0.03	0.20 ± 0.05	<0.03	<0.03	0.03
total	99.7	100.0	99.7	100.1	99.5	99.5	100.5	101.7	101.1
Fa		4.4						13.5 ± 3.7	31.6
Fs	2.3 ± 0.1		2.8 ± 0.1	7.1 ± 0.9	2.4 ± 0.0	2.7 ± 0.5	21.5		
Wo	0.3 ± 0.1		0.3 ± 0.1	0.4 ± 0.1	0.3 ± 0.1	41.0 ± 3.7	3.5		

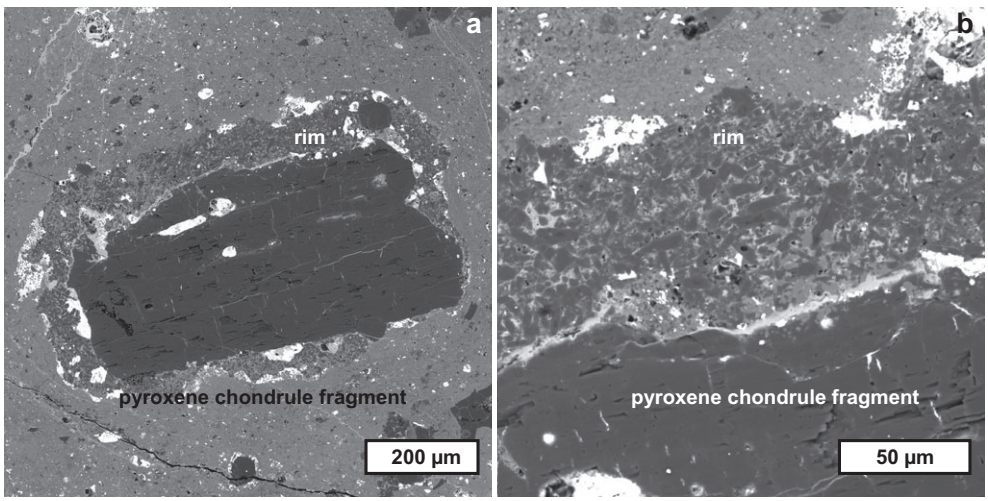

Fig. 5. Chondrule fragment consisting of elongated low-FeO low-Ca pyroxene grains surrounded by an igneous rim. a) Fragment and rim surrounded by matrix. b) Higher magnification image of the rim showing that it consists mainly of 5–10 µm sized low-Ca pyroxene and olivine grains. Many of the pyroxene grains are elongated with aspect ratios ranging up to 12:1; the olivine grains tend to be more equant. BSE images.

phenocrysts. The mesostasis in the chondrule is devitrified. Olivine (Fa4.4) and low-Ca pyroxene (Fs2.3Wo0.3) contain only minor FeO (Table 3).

Troilite in the clast occurs in a variety of petrographic settings (a) coarse grains (~10–75 µm) within chondrules between the phenocrysts, (b) discontinuous 5–25 µm thick sulfide rims around chondrules, (c) 80–160 µm sized rounded metal-sulfide globules containing 50–60 vol% polycrystalline troilite and 40–50 vol% metallic Fe-Ni (Fig. 7), (d) isolated grains up to 40 µm in size, and (e) tiny grains (~0.3 µm) embedded in the fine-grained silicate matrix material. In fact, some patches of matrix are completely opaque and contain ~30 vol% troilite.

CAI-1

CAI-1, the sole refractory inclusion in the clast, is 450 × 600 µm in size and has an irregular shape (Fig. 8). It constitutes 0.6 vol% of the clast. It is a simple spinel-pyroxene-olivine inclusion fragment similar to those in CM chondrites that have been subject to only minor aqueous alteration (i.e., QUE 97990 and Paris; Rubin 2007, 2015). The grains within the CAI range from ~2 to ~30 µm; some clusters of

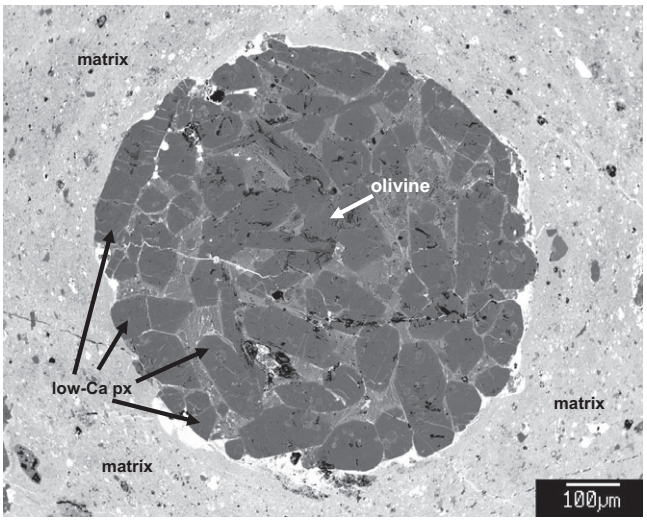

Fig. 6. Chondrule 1 is the largest chondrule, also visible in Fig. 2. It is a PP chondrule with a few small olivine grains. The devitrified mesostasis contains small Ca pyroxene crystallites. BSE image.

small (2–3 μm) grains have 120° triple junctions. Spinel grains tend to occur in 60–100 μm sized clusters scattered throughout the inclusion.

The mean FeO contents of the phases in CAI-1 are higher (and, in the case of spinel, much higher) than those in spinel-pyroxene-olivine inclusions or spinel inclusions in Paris—olivine: 2.9 ± 1.0 versus 0.76 ± 0.10 wt%; diopside: 0.73 ± 0.37 versus 0.63 ± 0.18 wt%; spinel: 10.9 ± 2.9 versus 0.63 ± 0.17 wt% (Table 4; Rubin 2015). This is not a primary distinction, but is a result of mild thermal metamorphism of the clast (see below).

AOI-1

There is a single amoeboid olivine inclusion in the clast (AOI-1); it is 95 × 115 μm in size (Fig. 9) and constitutes ~0.02 vol% of the clast. The AOI consists of major ferroan olivine, many grains with low-FeO cores and more-ferroan rims. Also present in the AOI are a few grains of low-FeO low-Ca pyroxene, diopside, and anorthite. Pores are 0.5–4 μm in size; they constitute ~4 vol% of the inclusion and are distributed throughout AOI-1.

Mineral Chemistry and Petrologic Type of Clast 6

Olivine and low-Ca pyroxene in the clast are unequilibrated (Fig. 10). Olivine ranges from Fa 4.2–31.6 with a mean composition of Fa 13.6 ± 5.9 (n = 68) and a percent mean deviation (PMD) of 32.8% (cf. Dodd et al. 1967) (Table 3). The highest-FeO olivines occur as isolated grains. Low-Ca pyroxene ranges from Fs 1.8–10.7 Wo 0.1–2.9 with a mean composition of Fs 4.3 ± 2.2 Wo 0.4 ± 0.3 (n = 72)

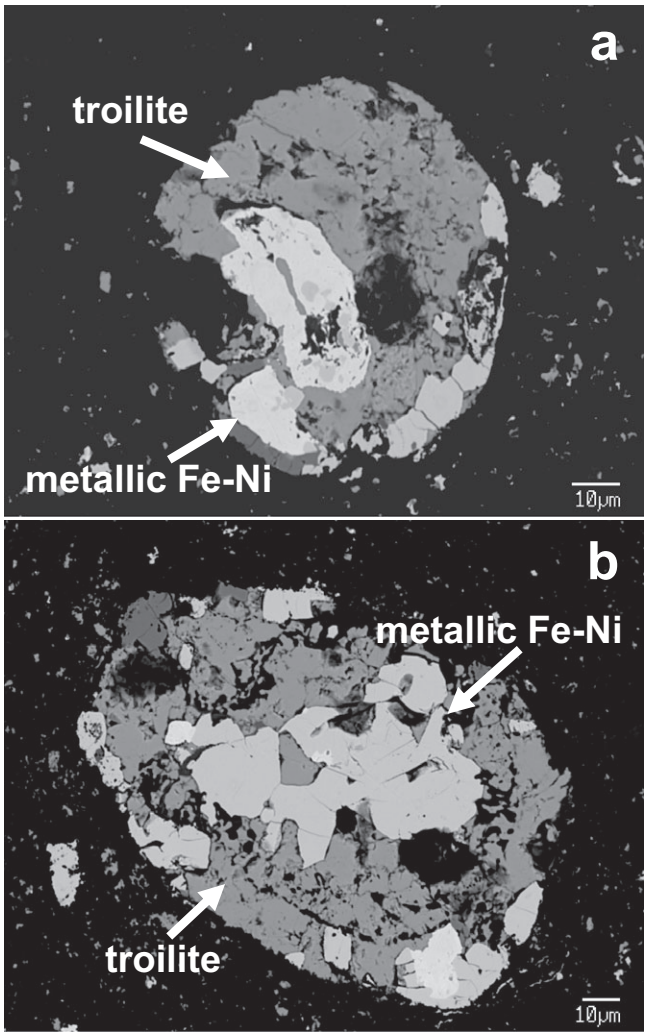

Fig. 7. Opaque globules from Clast 6. The assemblages consist mainly of troilite and metallic Fe-Ni. Some limonite, produced by terrestrial weathering, also occurs. a) Rounded globule consisting predominantly of troilite. b) Ellipsoidal globule containing subequal volumetric abundances of metal and sulfide. BSE images.

and a PMD of 40.3% (Table 3). Also present in the clast is high-Ca pyroxene: Fs2.7 ± 0.5 Wo41.0 ± 3.7 (n = 12) (Table 3). Although the classificatory data in table 1 of Huss et al. (2006) apply sensu stricto only to ordinary chondrites, this clast may be a new kind of ordinary chondrite (see below). The olivine data for Clast 6 correspond to petrologic subtype 3.4–3.5; the low-Ca pyroxene data correspond to subtype 3.0–3.6.

Opaque phases in the clast include kamacite with 2.6 ± 2.4 wt% Co, rare Ni-rich taenite (with ~50 wt% Ni), and troilite with concentrations of Ni and Cr marginally above the detection limit.

The chondrules in the clast contain devitrified mesostasis; none contain clear, isotropic glass (e.g., Fig. 6). This is characteristic of subtype 3.6–3.9. The

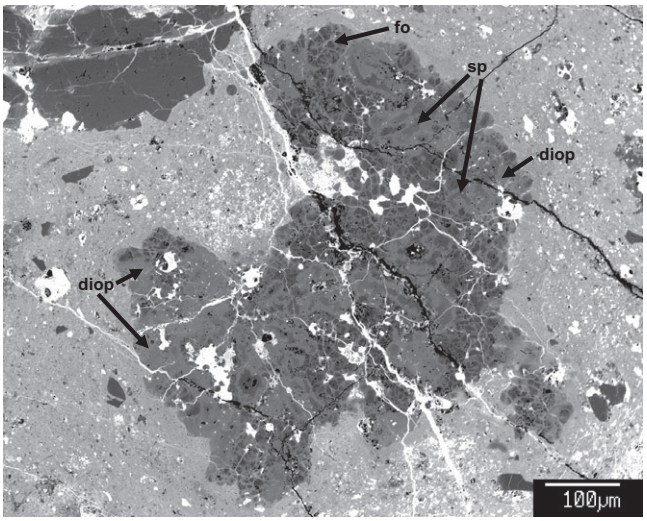

Fig. 8. CAI-1, the sole refractory inclusion in Clast 6. It is a simple spinel-pyroxene-olivine inclusion fragment similar to those in minimally altered CM chondrites. The most abundant phase is diopside; many spinel grains occur in 60–100 μm sized clusters throughout the inclusion. BSE image.

Table 4. Mean compositions (wt%) of silicate and oxide phases in refractory inclusion CAI-1 in Clast 6.

	Diopside	Olivine	Spinel
No. of analyses	5	12	21
SiO_2	50.8 ± 1.2	41.1 ± 0.3	0.08 ± 0.11
TiO_2	0.49 ± 0.46	<0.03	0.20 ± 0.07
Al_2O_3	4.7 ± 2.0	<0.03	67.9 ± 1.4
Cr_2O_3	0.05 ± 0.03	0.03 ± 0.02	0.51 ± 0.02
FeO	0.73 ± 0.37	2.9 ± 1.0	10.9 ± 2.9
MnO	<0.03	0.07 ± 0.03	0.07 ± 0.02
MgO	17.2 ± 1.0	55.9 ± 0.8	20.7 ± 2.5
CaO	24.7 ± 0.6	0.09 ± 0.02	0.13 ± 0.09
Na_2O	<0.03	<0.03	0.05 ± 0.06
Total	98.7	100.0	100.5
Fa		2.8 ± 1.0	
Fs	1.2 ± 0.6		
Wo	50.3 ± 2.1		

low-Ca pyroxene phenocrysts in the chondrules exhibit polysynthetic twinning, indicative of subtype ≤3.9.

Partial metamorphic equilibration is indicated by (a) olivine grains in the FeO-rich chondrule (Fig. 4) that consist typically of ferroan rinds surrounding less-ferroan cores, (b) forsterite grains in the CAI (Fig. 8) that are transected and surrounded by thin ferroan olivine veins and rims, and (c) the relatively high FeO contents of olivine and spinel in CAI-1. In addition, the small olivine grains in the matrix (Fig. 3) appear to be uniformly ferroan, consistent with equilibration and reflective of the high bulk FeO content of the fine-grained matrix material (37.6 wt%; Table 5).

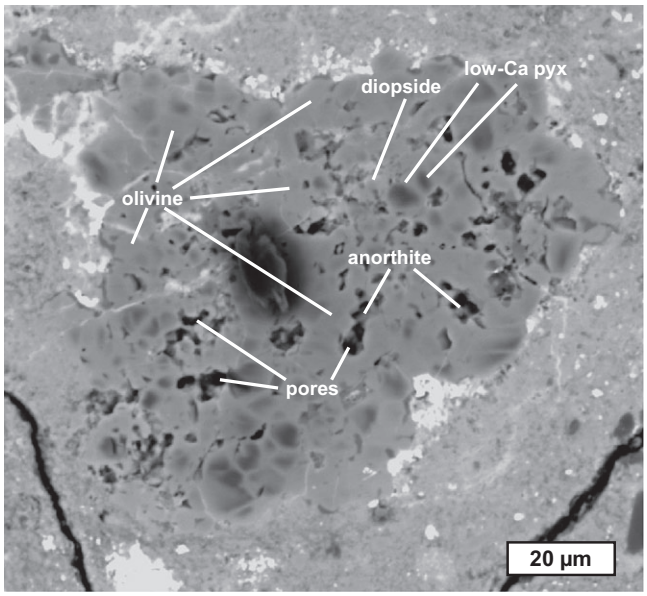

Fig. 9. AOI-1, the only amoeboid olivine inclusion in Clast 6, consists mainly of ferroan olivine. Also present are a few grains of low-FeO low-Ca pyroxene, anorthite, and diopside. Pores (black) are distributed throughout the inclusion. BSE image.

The extent of FeO enrichment around small low-FeO olivine grains in AOI-1 is intermediate between that in CO3.5 Lancé and CO3.6 ALH A77003 (fig. 7 of Chizmadia et al. 2002).

From these data, the best estimate for the subtype of Clast 6 is 3.6. This is within the range of the inferred subtype of the NWA 10214 host (3.6–3.9). However, there are several small low-FeO silicate grain fragments in the matrix of Clast 6 that are not surrounded by ferroan rims (e.g., center right of Fig. 3; center left of Fig. 8); it is possible that these grains were introduced into the clast after partial equilibration. They may be analogous to compositionally aberrant mineral grains in equilibrated OC (e.g., Rubin 1990).

The composition of the fine-grained matrix material in Clast 6 does not closely resemble those in the matrices in most other chondrite groups (Table 5). The Clast 6 matrix (e.g., Fig. 3) is richer in FeO (37.6 wt%) than the fine-grained opaque matrices in most type-3 ordinary chondrites (16.8–33.0 wt%; Huss et al. 1981), although the matrix in LL3 Krymka is exceptionally ferroan (42.8 wt% FeO). The FeO/MgO ratio in the matrix of Clast 6 (1.72) is closest to that of CO3 Kainsaz (1.77), but the SiO_2/MgO ratio in the matrix of Clast 6 (1.45) is closest to that in the $CV3_{red}$ Vigarano matrix sample (1.56). In contrast, EH3 matrix has much lower FeO/MgO (0.71) and much higher SiO_2/MgO (2.77) (Table 5).

Figure 11 shows that the matrix of Clast 6 is closest in composition to those in CV3 chondrites, particularly

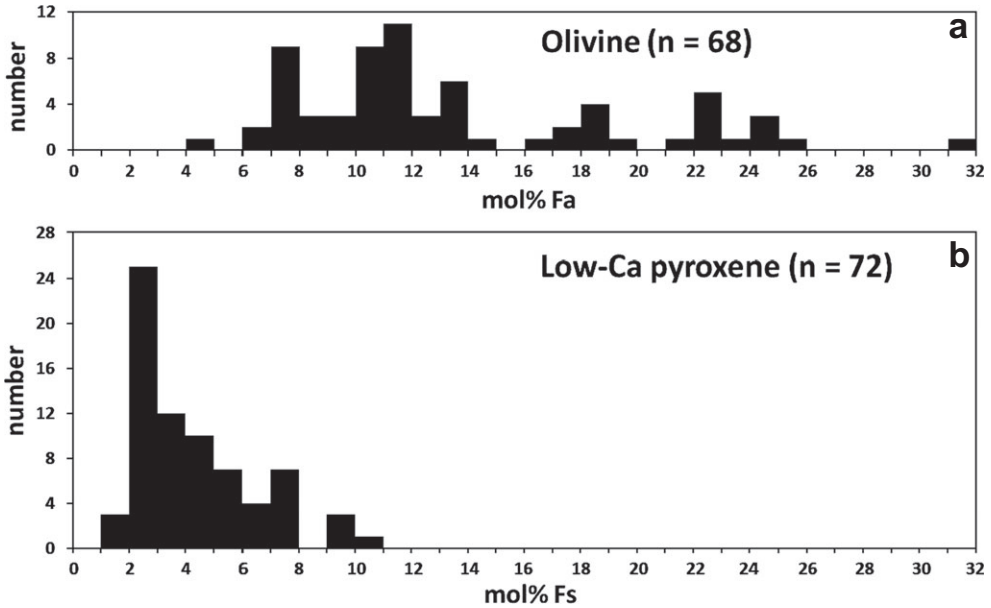

Fig. 10. a,b) Olivine and low-Ca pyroxene compositional distributions in Clast 6. The clast is unequilibrated and the minerals exhibit large grain-to-grain chemical variations. Low-Ca pyroxene peaks at relatively low Fs values.

Table 5. Mean composition (wt%) of fine-grained matrix material in Clast 6 and different chondrite groups.

	NWA 10214 LL3 Clast 6	Vigarano CV3-red fine fraction A	Allende CV3-ox matrix	Paris CM2 matrix	Parnallee LL3 opaque matrix	Krymka LL3 opaque matrix	Kainsaz CO3 matrix	Renazzo CR2 matrix	Y 691 EH3 matrix
Ref	1	2	3	4	5	5	6	6	7
Number	10	88	35	10	30	53	≥20	≥20	122
SiO_2	31.6 ± 2.5	27.0	29.6	27.1 ± 1.5	42.4	37.7	30.6	31.4	53.7
TiO_2	0.07 ± 0.04	nd	0.09	nd	0.10	0.07	0.10	0.07	nd
Al_2O_3	2.0 ± 0.8	2.0	1.7	2.5 ± 0.3	3.5	3.0	3.6	2.7	2.6
Cr_2O_3	0.39 ± 0.21	0.31	0.49	0.28 ± 0.05	0.43	0.30	0.35	0.35	0.22
FeO	37.6 ± 2.6	46.2	36.9	34.0 ± 2.0	22.5	42.8[a]	31.8	24.3	13.7
NiO	1.6 ± 0.8	nd	0.63	nd	0.13	0.64	1.1	1.5	0.23
MnO	0.36 ± 0.06	0.25	0.20	0.21 ± 0.04	0.33	0.39	0.33	0.33	0.09
MgO	21.8 ± 3.1	17.3	20.6	13.2 ± 1.2	23.3	13.0	18.0	15.8	19.4
CaO	0.86 ± 0.74	0.41	0.22	0.34 ± 0.21	1.5	1.2	1.9	0.87	0.78
Na_2O	0.15 ± 0.06	0.12	0.05	1.0 ± 0.2	1.9	0.91	0.49	1.2	1.3
K_2O	<0.04	<0.04	<0.04	0.08 ± 0.02	0.27	0.38	0.10	0.16	0.25
P_2O_5	0.29 ± 0.10	nd	0.15	nd	0.26	0.21	nd	nd	0.14
S	0.42 ± 0.52	1.8	0.45	4.2 ± 0.8	0.25	0.18	0.09	3.2	3.3
Total	97.1	95.4	91.1	80.9	96.9	100.8	88.5	81.9	95.7

References: 1 = this study; 2 = Hurt et al. (2012); 3 = Zolensky et al. (1993); 4 = Rubin (2015); 5 = Huss et al. (1981); 6 = McSween and Richardson (1977); 7 = Rubin et al. (2009). The Fe-Ni metal in the Parnallee and Krymka analyses were recalculated assuming an Fe/Ni ratio of 10:1. The low total in most of the matrix analyses reflects the presence of porosity and bound water.

[a]The Krymka matrix also contains 4.8 wt% metallic Fe; if this were added to the FeO concentration, the FeO would increase to 49.0 wt% and the matrix total would be 107.0 wt%.

nd = not determined.

Vigarano ($CV3_{red}$). Both have similar CI- and Mg-normalized abundance ratios of Al, Cr, Mn, Na, K, and S; Vigarano matrix is moderately richer in Fe and moderately depleted in Ca relative to the matrix of Clast 6.

The S content of fine-grained matrix material is generally high in the least-metamorphosed chondritic samples and low in the more-metamorphosed ones (e.g., Grossman and Brearley 2005; table 1 of Huss et al. 2006). For example, the matrix in LL3.00 Semarkona

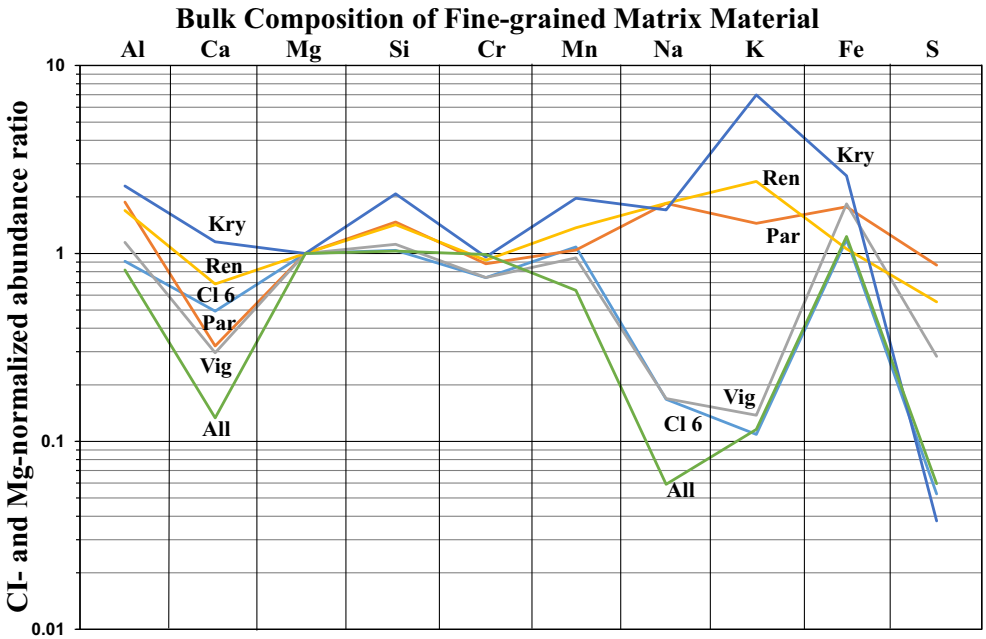

Fig. 11. Mean compositions of fine-grained matrix material in different chondrite groups normalized to CI chondrites and to Mg. The matrix in Clast 6 is closest to that in CV3 chondrites, particularly Vigarano. Kry = Krymka, LL3; Ren = Renazzo, CR2; CL 6 = Clast 6; Par = Parnallee, LL3; Vig = Vigarano, $CV3_{red}$; All = Allende, $CV3_{Ox}$. (Color figure can be viewed at wileyonlinelibrary.com.)

Table 6. Oxygen-isotopic compositions in Clast 6 and the NWA 10214 host.

	Object	Phase	$\delta^{18}O$ (‰)	$\delta^{17}O$ (‰)	$\Delta^{17}O$ (‰)
Clast 6	Chondrule 1	Low-Ca pyx	1.90	2.11	1.12
Clast 6	Chondrule 2	Low-Ca pyx	1.59	1.08	0.26
Clast 6	Chondrule 3	Low-Ca pyx	0.67	1.51	1.17
Clast 6	Chondrule 4	Low-Ca pyx	0.69	0.32	−0.03
Clast 6	Chondrule 4	Low-Ca pyx	0.70	0.44	0.08
Clast 6	CAI-1	Diopside	−44.78	−46.38	−23.09
Clast 6	CAI-1	Diopside	−44.42	−46.14	−23.04
Clast 6	CAI-1	Diopside	−47.67	−48.38	−23.59
NWA 10214 host	Chondrule	Low-Ca pyx	1.07	1.69	1.14
Standard	San Carlos	Olivine	5.02	2.91	0.30
Standard	San Carlos	Olivine	5.53	3.30	0.42
Standard	San Carlos	Olivine	5.43	2.76	−0.06
Standard	San Carlos	Olivine	5.11	2.73	0.07
Standard	San Carlos	Olivine	4.92	2.31	−0.25

contains 1.2 wt% S, whereas that in H/L3.6 Tieschitz contains only 0.08 wt% S (calculated from table 7 of Grossman and Brearley 2005). The S content of matrix also tends to be high in the least aqueously altered carbonaceous chondrites and low in the more altered chondrites (e.g., McSween and Richardson 1977; Rubin 2015). For example, the matrix in CM2.7 Paris (one of the least altered CM chondrites; Hewins et al. 2014; Marrocchi et al. 2014; Rubin 2015) contains 4.2 wt% S (Table 5), whereas that in CM2.2 Nogoya (a highly altered CM chondrite; Rubin et al. 2007) contains only 1.9 wt% S (McSween and Richardson 1977). The relatively low S content of matrix material in Clast 6 (0.42 wt%) is consistent with a moderately high petrologic subtype.

Oxygen-Isotopic Compositions

Oxygen-isotopic compositions are listed in Table 6. The 1 σ reproducibility of the San Carlos olivine standard is $\delta^{17}O = 0.4‰$; $\delta^{18}O = 0.3‰$; it forms a tight cluster along the terrestrial fractionation (TF) line

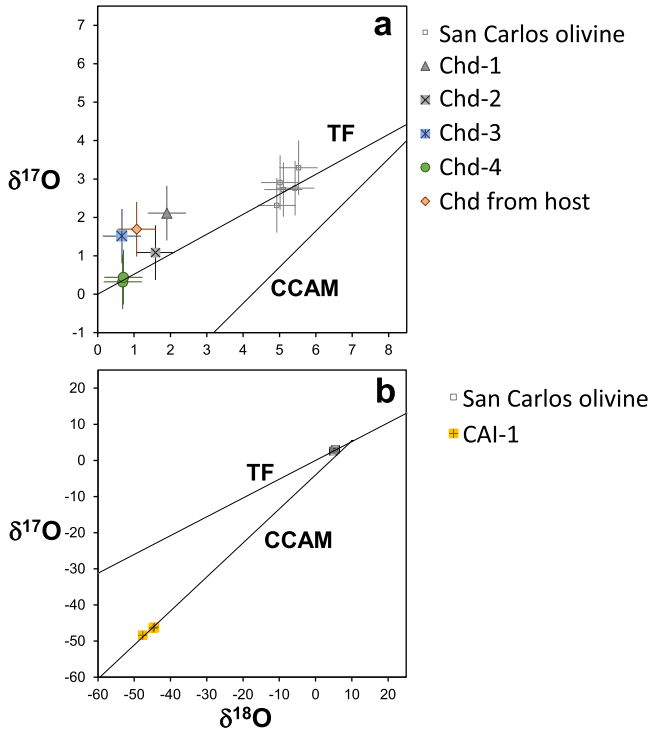

Fig. 12. O-isotopic compositions displayed in the standard three-isotope diagram. Uncertainties are plotted as 2σ. a) San Carlos olivine standard and chondrules from Clast 6 as well as one from the NWA 10214 host. The compositions of low-Ca pyroxene grains in the chondrules are similar to those of literature values for many LL3 chondrules. The San Carlos olivine standards fall along the terrestrial fractionation (TF) line. b) Diopside grains in CAI-1 have O-isotopic compositions near $\delta^{17}O = -45‰$; $\delta^{18}O = -46‰$; $\Delta^{17}O = -23‰$; they lie along the carbonaceous-chondrite anhydrous minerals (CCAM) mixing line and in the vicinity of many literature values for CAI phases. Also shown are the San Carlos olivine standards. (Color figure can be viewed at wileyonlinelibrary.com.)

(Fig. 12a). This indicates that the O-isotopic analyses are precise and accurate; plotted uncertainties are 2σ.

There is a fairly tight cluster of points centered near $\delta^{17}O = \sim 1.0‰$; $\delta^{18}O = \sim 1.0‰$ (Fig. 12a) that includes low-Ca pyroxene in four chondrules from Clast 6 as well as one chondrule from outside the clast, that is, in the NWA 10214 host. This cluster occurs along and just above the TF line and is near the ^{16}O-rich end of the field of olivine and pyroxene from LL3.0–3.1 chondrules measured by Kita et al. (2010); it is also within the range of chondrules in R3 clasts in R-chondrite breccias measured by Kita et al. (2015) and in the vicinity of chondrules from type-3 enstatite chondrites (Weisberg et al. 2011). The Clast 6 chondrules have a mean $\Delta^{17}O$ value of $0.5 \pm 0.6‰$ ($n = 5$); the LL3 chondrules have a mean $\Delta^{17}O$ value of $0.56 \pm 0.45‰$ ($n = 37$; excluding one ^{16}O-rich chondrule) (Kita et al. 2010). The O-isotope data are consistent with a scenario in which the chondrule from the NWA 10214 host and the chondrules from Clast 6 were all derived from the same O-isotopic reservoir as OC chondrules.

In contrast, diopside from CAI-1 (Fig. 12b) has an O-isotopic composition near $\delta^{17}O = -45‰$; $\delta^{18}O = -46‰$; $\Delta^{17}O = -23‰$, along the carbonaceous-chondrite anhydrous minerals (CCAM) mixing line. It is very similar in composition to that of mafic silicates in many unaltered CAIs from primitive chondritic meteorites (e.g., MacPherson 2005).

DISCUSSION

Classification of Clast 6

Clast 6 has some properties broadly resembling those of carbonaceous chondrites, ordinary chondrites, and enstatite chondrites (Table 7). Some polymict breccias such as Kaidun (e.g., Zolensky and Ivanov 2003) and Almahata Sitta (e.g., Bischoff et al. 2010) contain discrete clasts of different chondrite groups. The Y 82094 ungrouped carbonaceous chondrite has a low abundance of matrix (11.1 vol%), similar to that in ordinary (10–15 vol%) and enstatite (8–10 vol%) chondrites (Kimura et al. 2014). However, no single meteoritic lithology yet described has such peculiar characteristics as Clast 6.

Carbonaceous Chondrite-Like Properties

(a) The modal abundance of matrix material in Clast 6 is ~60 vol% (Fig. 2). The only major chondrite group with 60 vol% matrix is CM (Wasson 2008; Rubin 2010). CO3, CV3, and CR2 chondrites contain less matrix (with mean modal abundances of 34, 35, and 42 vol%, respectively; McSween 1977a, 1977b; Weisberg et al. 1993). R chondrites average 42 ± 11 vol% matrix (Rubin and Kallemeyn 1993); some R3 clasts in R-chondrite breccias contain ~50 vol% matrix (Bischoff 2000). Type-3 ordinary and enstatite chondrites contain only 8–12 vol% matrix (Huss et al. 1981; Rubin et al. 2009; Rubin 2010). CI chondrites constitute the only major group that contains more matrix—nearly 100 vol% (including ~10 vol% embedded magnetite grains; e.g., McSween 1979). On the other hand, several individual clasts in ordinary chondrites are matrix rich; these include a fine-grained matrix-like cognate dark inclusion in Tieschitz (Dobrică and Brearley 2014), a microchondrule-bearing dark clast with 52 vol% matrix in Rio Negro (Fodor et al. 1977; Rubin 1982), a microchondrule-bearing clast with 80 vol% matrix in Krymka (Rubin 1989), and millimeter-sized lumps of matrix material in several OC (e.g., Ikeda et al. 1981; Scott et al. 1984). (b) The composition of the matrix in

Table 7. Physical properties of Clast 6 compared to mean properties of other chondrite groups.

Chondrite group	Clast 6	CM	CO	CV	CR	R	H	L	LL	EH	EL
Matrix abundance (vol%)	60[a]	60[b]	34[b]	35[b]	42[c]	42[b]	12[b]	12[b]	12[b]	8[b]	10[b]
Mean chondrule diameter (μm)	330[a]	270[d]	150[d]	900[d]	700[d]	400[d]	450[d]	500[d]	550[d]	230[d]	500[d]
RP+C chondrules (%)	0[a]	1.6[d]	3[d]	0.3[d]	0.7[d]	1.6[d]	7[d]	7[d]	7[d]	18[d]	13[d]
CAI abundance (vol%)	0.6[a]	1.2[b]	1.0[b]	3.0[b]	0.6[b]	0.04[b]	0.02[b]	0.02[b]	0.02[b]	0.01[b]	0.01[b]
Chondrules with igneous rims (%)	0[a]	0.1[d]	0.1[d]	50[d]	26[d]	0.8[d]	10[d]	10[d]	10[d]	0.2[d]	0.3[d]
Low-Ca px/olivine ratio	4[a]	0.14[e]	0.13[e]	0.07[f]	0.40[g]	0.06[h]	0.7[i]	0.5[i]	0.3[i]	14[j]	27[j]
Metallic Fe-Ni (vol%)	0.1[a]	0.2[k]	2.5[m]	CV_{red}: 2.5[n] CV_{ox}: 0.1[n]	6.7[p]	0.04[q]	8.4[r]	4.1[r]	2.0[r]	9.3[j]	10.1[j]

References: a = this study; b = Rubin (2011) wherein the data for ordinary chondrites are assumed to be the same for matrix abundance and CAI abundance; c = Rubin and Kallemeyn (1993); d = Friedrich et al. (2015) and Rubin (2010); the three OC groups are assumed to all have the same percentages of RP+C chondrules and chondrules with igneous rims; e = CIPW norms (vol%) of Jarosewich (1990) data for CM Murchison and CO ALH 77003; f = Tomeoka et al. (2005) data for CK4 Kobe, assumed to be representative of equilibrated CV3 chondrites; g = CIPW norm (vol%) of Mason and Wiik (1962) data for CR Renazzo; h = Kallemeyn et al. (1996); i = table 5.1 of Hutchison (2004); j = Weisberg and Kimura (2012); k = Rubin et al. (2007); m = McSween (1977a); n = McSween (1977b) of reduced CV chondrites (CV_{red}) and oxidized CV chondrites (CV_{ox}); p = Weisberg et al. (1993); q = Bischoff et al. (2011); r = Krot et al. (2005).

Clast 6 is closest to that of the matrix in Vigarano ($CV3_{red}$) (Fig. 11). (c) The modal abundance of CAIs in Clast 6 is 0.6 vol%. Carbonaceous chondrites (other than the highly altered CI chondrites) contain 0.6–3.0 vol% CAIs; ordinary, enstatite, and R chondrites contain far fewer CAIs, that is, 0.01–0.04 vol% (table 2 of Rubin 2011). It would be very unlikely to find a moderate-size CAI in a random 26 mm^2 region of a noncarbonaceous chondrite. (d) The textural variety of the sole CAI in Clast 6 is spinel-pyroxene-olivine (Fig. 8), identical to one of the major varieties in minimally altered CM chondrites (Rubin 2007, 2015). (e) Clast 6 contains an AOI (Fig. 9) that constitutes ~0.02 vol% of the clast. This modal abundance is at least four times greater than that of AOIs in OC (Rubin 2011).

Ordinary Chondrite-Like Properties

The olivine and low-Ca pyroxene compositional distributions of Clast 6 (Fig. 10) most closely resemble those in partially equilibrated type-3 ordinary chondrites (e.g., H/L3.6 Tieschitz; fig. 1 of Dodd et al. 1967) (a) the olivine distributions are relatively flat with no large peaks at low Fa values and (b) the low-Ca pyroxene distributions have higher proportions of low-FeO grains and do not extend as far to higher FeO values. In contrast, carbonaceous chondrites tend to have large peaks at low Fa values (see below).

Berlin et al. (2011) found that the mean Fe/Mn ratio of olivines within Type-IIA chondrules differs between ordinary chondrites (Fe/Mn = 44) and CO carbonaceous chondrites (Fe/Mn = 99). The mean Fe/Mn ratio of isolated ferroan olivines (presumably derived from fragmented Type-IIA chondrules) in Clast 6 is 45 ± 18 (n = 6), nearly identical to that in OC.

The mean chondrule size in Clast 6 (330 ± 160 μm; n = 28) is within 1σ of that of H-group ordinary chondrites (~450 μm) or R chondrites (400 μm) (table 7 of Friedrich et al. 2015). Carbonaceous-chondrite and enstatite-chondrite chondrules tend to be either somewhat smaller (CM, 270 μm; CO, 150 μm; EH, 230 μm) or moderately larger (CV, 900 μm; CR, 700 μm; EL, 500 μm) (table 5 of Rubin 2010; table 7 of Friedrich et al. 2015).

The O-isotopic composition of the chondrules in Clast 6 are in the range of LL3 chondrules and have $\Delta^{17}O$ values ≳0‰ (Table 6; Fig. 12). The vast majority of chondrules from carbonaceous chondrites plot below the TF line on the standard three-isotope graph with $\Delta^{17}O$ values <0‰ (e.g., fig. 1 of Rubin 2000). There are no available O-isotope data for the matrix of Clast 6 or for the entire clast.

A distinctive property of Clast 6 is the high low-Ca pyroxene/olivine mean modal ratio in the chondrules (4:1), for example, Fig. 6. Ordinary, carbonaceous, and R chondrites are dominated by olivine-rich chondrules (e.g., Grossman et al. 1988; Rubin and Kallemeyn 1994). For example, Nelson and Rubin (2002) found that LL3 chondrites contain 47% POP+PPO, 21% PP, 16% PO, 6% BO, 3% RP, 4% C, and 3% GOP chondrules. Our unpublished observations of Semarkona chondrules indicate that there are about equal numbers of POP and PPO chondrules. Thus, about 45% of LL3 chondrules are PPO or PP. In contrast, Clast 6 contains 86% PPO or PP chondrules. A χ^2 test (with the Yates' correction for continuity) shows that the probability of 24/28 randomly chosen LL3 chondrules being PPO or PP is <0.0001, that is, less than one chance in 10,000. For this test, which assumes that the LL3 chondrule population is infinite, χ^2 = 17.1 with 1 degree of freedom. This mitigates against the likelihood that the chondrules in Clast 6 were derived from a normal LL3 chondrite.

Enstatite Chondrite-Like Properties

Enstatite chondrites contain mainly pyroxene-rich chondrules; a study of 689 EH3 chondrules in thin section identified 4% PPO+POP+PO, 77% PP, 13% RP, 5% C, and 1% GP (granular pyroxene) chondrules (Rubin and Grossman 1987). BO chondrules are very rare in type-3 enstatite chondrites (e.g., Nakamura-Messenger et al. 2012). The low-Ca pyroxene/olivine modal abundance ratio in chondrules and chondrule fragments as well as the FeO content of pyroxene in Clast 6 are closest to those in type-3 enstatite chondrites. However, the absence of nonporphyritic chondrules (RP, C, and GP types) in Clast 6 clearly distinguishes it from EH3 chondrites (in which 19% of the chondrules are nonporphyritic; Rubin and Grossman 1987).

Pyroxene grains in EH3 chondrules typically have low concentrations of FeO: 0.30–1.5 wt% (table 1 of Grossman et al. 1985), but a few more-ferroan grains (with up to 12 wt% FeO) are also present (Weisberg and Kimura 2012). Pyroxene in the chondrules in Clast 6 contain 1.6–5.0 wt% FeO, but one isolated pyroxene grain (probably derived from a fragmented chondrule) contains 14.1 wt% FeO (Table 3).

The mean minor element concentrations in low-Ca pyroxene within chondrules in Clast 6 (Table 3, n = 13) are similar to those in type-3 enstatite chondrites (table 1 of Weisberg et al. 2011, n = 12) (in wt%): Al_2O_3 (0.24 versus 0.33 ± 0.26); Cr_2O_3 (0.51 versus 0.37 ± 0.31); FeO (2.5 versus 2.3 ± 3.9); MnO (0.25 versus 0.16 ± 0.12); CaO (0.18 versus 0.34 ± 0.20).

Origin of Clast 6

The NWA 10214 host is clearly a brecciated LL3 chondrite (Fig. 1), whereas Clast 6 (Fig. 2) has a

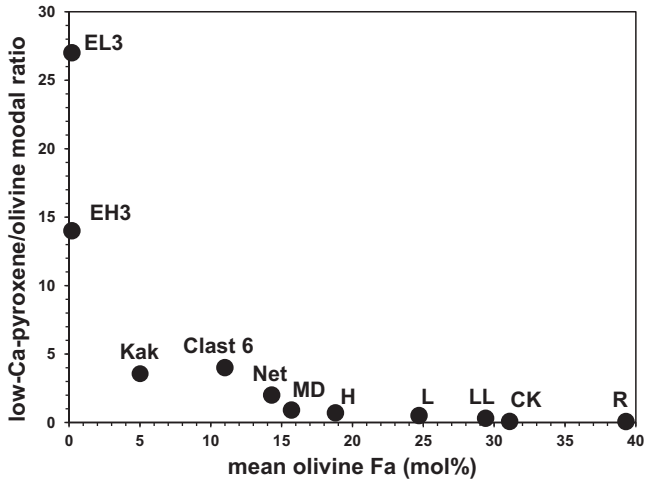

Fig. 13. Diagram showing that the low-Ca pyroxene/olivine modal ratio in chondritic materials decreases roughly exponentially with increasing mean olivine Fa content. Clast 6 lies close to the trend that ranges from the most reduced chondritic meteorites (EH and EL chondrites) to the most oxidized group (R chondrites). Because olivine grains in Clast 6 are largely unequilibrated (Fig. 10a), the Fa value plotted here (11 mol%) is the center of the peak of the olivine compositional distribution. MD = chondritic clasts in the Mont Dieu IIE iron; Net = chondritic clasts in the Netschaevo IIE iron; Kak = Kakangari.

different provenance. Because neither Clast 6 nor the host is appreciably shocked, it seems likely that the clast is a fragment of a projectile that collided with the LL parent asteroid at low relative velocity. The significant amount of chondrule fragments in Clast 6 points to a history of comminution; this process of impact fragmentation could have taken place at any stage in its history.

As described above, the O-isotopic compositions of chondrules in Clast 6 (Fig. 12) match those of OC chondrules. In addition, the mean size of the chondrules in the clast (330 ± 160 μm) is within one standard deviation of the mean size of H-chondrite chondrules (450 μm; Friedrich et al. 2015). Therefore, a possible origin for the clast is that it was an H3 chondrite that acquired a much greater-than-normal allotment of matrix material. This scenario is not farfetched: R chondrites closely resemble ordinary chondrites except for having an unusually high abundance of ^{17}O-rich, bound-water-bearing matrix material (e.g., Kallemeyn et al. 1996; Rubin 2010, 2014; Bischoff et al. 2011). Even the chondrules in R3 chondrite clasts have O-isotopic compositions overlapping the range of LL3 chondrules (Kita et al. 2010, 2015).

A viable model for the origin of Clast 6 must also account for the clast's relatively high CAI modal abundance (0.6 versus ~0.02 vol% in typical OC; Table 7). The correspondence between a high matrix abundance and a high CAI abundance in a chondrite may be a result of radial drift processes in the solar nebula that affected porous multi-millimeter-to-centimeter-sized dustballs (i.e., matrix precursors) to about the same extent as smaller, more-compact CAIs (Rubin 2011). The rate of radial drift in the nebula is a function of the product of the size and density of an entrained object (e.g., Weidenschilling 1977; Nakagawa et al. 1986). Large porous dustballs made of matrix material and smaller, dense CAIs would be aerodynamically concentrated in the same nebular regions (Rubin 2011). Dustballs (like the one that gave rise to the matrix of Clast 6), CAIs (physically similar to CAI-1), and AOIs (similar to AOI-1) may have independently drifted to the particular portion of the OC nebular region where the clast's precursor agglomerated. This scenario is consistent with the positive correlation among chondrite groups between the modal abundances of matrix and CAIs (fig. 4 of Rubin 2011).

The other anomalous characteristic of Clast 6 is the high low-Ca pyroxene/olivine modal ratio in the clast's chondrules and chondrule fragments: 4:1. Among the major chondrite groups, high low-Ca pyroxene/olivine ratios are found only in enstatite chondrites. This is because so little of the metallic Fe in these reduced rocks has been oxidized to FeO that the ratio of divalent cations to Si remains close to unity (as in $MgSiO_3$), stabilizing low-Ca pyroxene. In more-oxidized chondrites (with higher FeO), the divalent-cation/Si ratio climbs toward 2 (as in $(Mg,Fe)_2SiO_4$), stabilizing olivine.

With increasing degrees of reduction, the low-Ca pyroxene/olivine modal ratio in chondritic materials increases (Fig. 13). R chondrites comprise the most oxidized non-CI group with a mean low-Ca pyroxene/olivine modal ratio of 0.06 (table 2 of Kallemeyn et al. 1996, excluding the minimally equilibrated R3.6 ALH 85151) and an assumed olivine Fa content identical to that in R3.8 Carlisle Lakes (39.3 mol%; Rubin and Kallemeyn 1989). CK4 Kobe is assumed here to represent CK chondrites (or equilibrated CV chondrites; Greenwood et al. 2010; Wasson et al. 2013); Kobe has a low-Ca pyroxene/olivine modal ratio of 0.07 and a mean olivine Fa content of 31.1 mol% (Tomeoka et al. 2005). In ordinary chondrites, the low-Ca pyroxene/olivine modal ratio is 0.3 in LL (mean Fa 29.4 mol%), 0.5 in L (mean Fa 24.7 mol%) and 0.7 in H (mean Fa 18.8 mol%) (table 5.1 of Hutchison 2004; table 3 of Rubin 1990).

Chondrule-bearing silicate clasts in the Mont Dieu IIE iron are more reduced than H chondrites, but plausibly are still members of the ordinary-chondrite clan. The low-Ca pyroxene/olivine modal ratio in the Mont Dieu clasts is 0.9 (mean Fa 15.7 mol%) (Van Roosbroek et al. 2015). Chondritic clasts in the IIE iron

Netschaevo also appear to be members of the OC clan and are even more reduced (Bild and Wasson 1977; Rubin 1990). The low-Ca pyroxene/olivine modal ratio in the Netschaevo clasts is 2.0 (mean Fa 14.3 mol%) (table 3 of Olsen and Jarosewich 1971; Rubin 1990). The ungrouped, unequilibrated chondrite Kakangari is more reduced than Netschaevo (mean Fa 5 mol%; table 1 of Graham et al. 1977); its low-Ca pyroxene/olivine modal ratio is 3.6 (table 2 of Weisberg et al. 1996). Clast 6 is intermediate between Netschaevo and Kakangari in its degree of reduction (Fig. 13). The most reduced chondritic materials are enstatite chondrites. EH3 and EL3 chondrites have low-Ca pyroxene/olivine modal ratios of 14 and 27, respectively (table 3 of Weisberg and Kimura 2012); for plotting purposes, the mean olivine Fa content in each of these groups is assumed to be 0.2 mol% (the value in a chondrule from EH4 QUE 94368; Rubin 1997). (EH3 and EL3 chondrites must be used in this analysis because type-4–6 enstatite chondrites are olivine free [Mason 1966; Keil 1968].) The smooth, roughly exponential trend illustrates the strong relationship between oxidation state and the low-Ca pyroxene/olivine ratio among chondritic samples.

Matrix-rich chondrite groups that have equilibrated members are oxidized; these include R chondrites (42 vol% matrix, Fa 39.3) and CK chondrites (50 vol% matrix, Fa31.1) (Rubin and Kallemeyn 1993; table 2 of Rubin 2011; this study). More reduced chondrite groups (i.e., ordinary and enstatite chondrites) have much lower abundances of matrix material (8–12 vol%; Rubin 2011), although this set includes LL chondrites which are nearly as oxidized as CK chondrites (e.g., Fa 29.4 versus 31.1). Clast 6 does not follow this general trend; it is a reduced, matrix-rich chondritic sample. Although ordinary and R chondrite whole rocks may have been oxidized by reactions with OH-bearing matrix-like dust (e.g., Rubin 2005), the dust that agglomerated with the progenitors of Clast 6 was probably depleted in OH-bearing phases.

A comparison of the olivine and low-Ca pyroxene histograms in Clast 6 (Fig. 10) shows that there are many ferroan olivine grains (i.e., 50/68 with Fa values >10 mol%) and very few ferroan low-Ca pyroxene grains (i.e., 1/72 with Fs values >10 mol%). This is analogous to the olivine and low-Ca pyroxene compositional distributions in many unequilibrated ordinary, carbonaceous, and R chondrites: for example, type-3 ordinary chondrites (fig. 1 of Dodd et al. 1967); CO3.0 Colony (fig. 3a,b of Rubin et al. 1985); CV3 chondrites (Van Schmus 1969); CM2 chondrites (fig. 1 of Wood 1967; fig. 10 of Fuchs et al. 1973); the Acfer 187 and EET 87770 CR chondrites and their paired specimens (fig. 5 of Bischoff et al. 1993; fig. 1 of Kallemeyn et al. 1994), and unequilibrated R-chondrite clasts in the DaG 013 and Hughes 030 R3–6 breccias (figs. 6, 7 of Bischoff 2000).

Figure 1 of Frank et al. (2014) shows the compositional distribution of 72 isolated 5–30 μm size olivine grains in the matrices of LL3.00 Semarkona and L3.05 QUE 97008. There is a large peak at Fa~1 and a broad peak at Fa~19–29. This distribution is similar (but not identical) to that of 346 small olivine grains from chondrules and chondrule fragments in Semarkona (fig. 2c of Takagi 2005) that shows a large peak at Fa~1 and a broad peak at Fa~21–34. (The olivine compositional distribution in LL3.00 Semarkona more closely resembles those in carbonaceous chondrites than those of more-equilibrated type-3 OC such as LL3.15 Bishunpur, LL3.2 Krymka, L3.4 Hallingeberg, or H/L3.6 Tieschitz [Dodd et al. 1967].) The general similarity between the distributions in Semarkona and the matrix olivine grains analyzed by Frank et al. (2014) suggests that the latter grains are actually chondrule fragments. In contrast, olivine grains that appear to have been derived from nebular dust and now occur within the matrices of type-3 OC tend to be much finer grained, that is, <0.1 μm (Alexander et al. 1989; Brearley et al. 1989) and have highly variable Fa contents, that is, Fa~1–91 (Nagahara 1984).

These data support the conclusion that the relatively coarse (>5 μm) FeO-bearing grains in all of these chondrites and in Clast 6 are derived from fragmented ferroan chondrules. These chondrules tend to have high olivine/low-Ca pyroxene ratios because, as discussed above, they have high divalent-cation/Si ratios, favoring the crystallization of olivine [$(Mg,Fe)_2SiO_4$] over low-Ca pyroxene $(Mg,Fe)SiO_3$. That is why the olivine compositional distributions generally extend to much higher FeO values than the corresponding low-Ca pyroxene distributions.

However, the olivine compositional distributions in carbonaceous chondrites (e.g., Wood 1967; Van Schmus 1969; Fuchs et al. 1973; Rubin et al. 1985; Bischoff et al. 1993; Kallemeyn et al. 1994) tend to have very high peaks at very low Fa values, indicative of the large proportions of Type-IA chondrules in these rocks. R chondrites and type-3 OC (save Semarkona) tend to have lower proportions of these chondrules and consequently have lower peaks at very low Fa contents in their olivine compositional distributions (e.g., Dodd et al. 1967; Bischoff 2000; Kita et al., 2010, 2013). Clast 6 lacks Type-IA chondrules and thus does not have a high peak at low Fa contents in its olivine compositional distribution (Fig. 10).

Clast 6 can thus be modeled as a type-3 ordinary chondrite, somewhat more reduced than H chondrites or the chondritic clasts in the Netschaevo IIE iron, but less reduced than Kakangari or enstatite chondrites. The

material that agglomerated to produce the parent asteroid of the clast formed in a nebular region where aerodynamic radial drift processes had deposited a relatively high abundance of matrix material, CAIs, and AOIs. At some point, a collision launched material off this asteroid; some of it eventually impacted the LL-chondrite parent body at low relative velocity. A fragment of this projectile became Clast 6. Along with shocked and metamorphosed clasts derived from different regions of the LL asteroid, Clast 6 was incorporated into previously unconsolidated LL3 material. The entire assemblage was subsequently lithified by impact-induced compaction; the clast was mildly metamorphosed along with the NWA 10214 LL-chondrite host. This mild metamorphism is indicated by (a) the ferroan rinds and veins around grains in the FeO-rich chondrule (Fig. 4), CAI (Fig. 8), and AOI (Fig. 9); (b) the uniformly high FeO content of fine-grained olivine in the matrix (e.g., Fig. 3); and (c) the relatively ferroan compositions of olivine and spinel in the CAI. Nevertheless, recrystallization and textural integration were minimal, leaving the clast/host boundary sharp. The small low-FeO mafic silicate grains in the matrix lack ferroan rims (Figs. 3, 4, 6, 8, 9), consistent with postmetamorphic fragmentation, incorporation of minor amounts of nearby type-3 chondritic debris, and impact-induced recompaction of the clast.

Although there are many ungrouped carbonaceous chondrites (e.g., Davy et al. 1978; Kallemeyn and Rubin 1995; Newton et al. 1995; Choe et al. 2010; Kimura et al. 2014; Meteoritical Bulletin Database), there are few ungrouped ordinary chondrites (if meteorites classified as H/L and L/LL are considered grouped). The principal exceptions are reduced samples such as the Netschaevo and Mount Dieu IIE irons and Clast 6.

Acknowledgments—We thank J. T. Wasson for useful comments and M. K. Weisberg, A. Bischoff, J. N. Bigolski, and A. J. Brearley for helpful reviews. Associate editor M. E. Zolensky also provided useful suggestions. This research was supported by NASA Grant NNG06GF95G (AER).

Editorial Handling—Dr. Michael Zolensky

REFERENCES

Alexander C. M. O'D., Hutchison R., and Barber D. J. 1989. Origin of chondrule rims and interchondrule matrices in unequilibrated ordinary chondrites. *Earth and Planetary Science Letters* 95:187–207.

Berlin J., Jones R. H., and Brearley A. J. 2011. Fe-Mn systematics of type IIA chondrules in unequilibrated CO, CR, and ordinary chondrites. *Meteoritics & Planetary Science* 46:513–533.

Bild R. W. and Wasson J. T. 1977. Netschaevo: A new class of chondritic meteorite. *Science* 197:58–62.

Bischoff A. 2000. Mineralogical characterization of primitive, type-3 lithologies in Rumuruti chondrites. *Meteoritics & Planetary Science* 35:699–706.

Bischoff A., Palme H., Ash R. D., Clayton R. N., Schultz L., Herpers U., Stöffler D., Grady M. M., Pillinger C. T., Spettel B., Weber H., Grund T., Endreβ M., and Weber D. 1993. Paired Renazzo-type (CR) carbonaceous chondrites from the Sahara. *Geochimica et Cosmochimica Acta* 57:1587–1603.

Bischoff A., Horstmann M., Pack A., Laubstein M., and Haberer S. 2010. Asteroid 2008 TC_3 – Almahata Sitta: A spectacular breccia containing many different ureilitic and chondritic lithologies. *Meteoritics & Planetary Science* 45:1638–1656.

Bischoff A., Vogel N., and Roszjar J. 2011. The Rumuruti chondrite group. *Chemie der Erde* 71:101–133.

Brearley A. J. 1990. Carbon-rich aggregates in type 3 ordinary chondrites: Characterization, origins and thermal history. *Geochimica et Cosmochimica Acta* 54:831–850.

Brearley A. J., Scott E. R. D., Keil K., Clayton R. N., Mayeda T. K., Boynton W. V., and Hill D. H. 1989. Chemical, isotopic and mineralogical evidence of the origin of matrix in ordinary chondrites. *Geochimica et Cosmochimica Acta* 53:2081–2093.

Chizmadia L. J., Rubin A. E., and Wasson J. T. 2002. Mineralogy and petrology of amoeboid olivine inclusions in CO3 chondrites: Relationship to parent-body aqueous alteration. *Meteoritics & Planetary Science* 37:1781–1796.

Choe W. H., Huber H., Rubin A. E., Kallemeyn G. W., and Wasson J. T. 2010. Compositions and taxonomy of 15 unusual carbonaceous chondrites. *Meteoritics & Planetary Science* 45:531–554.

Davy R., Whitehead S. G., and Pitt G. 1978. The Adelaide meteorite. *Meteoritics* 13:121–140.

Dobrică E. and Brearley A. J. 2014. Widespread hydrothermal alteration minerals in the fine-grained matrices of the Tieschitz unequilibrated chondrite. *Meteoritics & Planetary Science* 49:1323–1349.

Dodd R. T. and Van Schmus W. R. 1971. Dark-zoned chondrules. *Chemie der Erde* 30:59–69.

Dodd R. T., Van Schmus W. R., and Koffman D. M. 1967. A survey of the unequilibrated ordinary chondrites. *Geochimica et Cosmochimica Acta* 31:921–951.

Fodor R. V. and Keil K. 1978. Catalog of lithic fragments in LL-group chondrites. *Special Publication University of New Mexico Institute of Meteoritics* 19:1–38.

Fodor R. V., Keil K., Wilkening L. L., Bogard D. D., and Gibson E. K. 1976. Origin and history of a meteorite parent-body regolith breccia: Carbonaceous lithic fragments in the Abbott, New Mexico, chondrite. *Special Publications of the New Mexico Geological Society* 6:206–218.

Fodor R. V., Keil K., and Gomes C. B. 1977. Studies of Brazilian meteorites IV. Origin of a dark-colored, unequilibrated lithic fragment in the Rio Negro chondrite. *Revista Brasileira de Geociências* 7:45–57.

Frank D. R., Zolensky M. E., and Le L. 2014. Olivine in terminal particles of Stardust aerogel tracks and analogous grains in chondrite matrix. *Geochimica et Cosmochimica Acta* 142:240–259.

Friedrich J. M., Weisberg M. K., Ebel D. S., Biltz A. E., Corbett B. M., Iotzov I. V., Khan W. S., and Wolman M.

D. 2015. Chondrule size and related physical properties: A compilation and evaluation of current data across all meteorite groups. *Chemie der Erde* 75:419–443.

Fuchs L. H., Olsen E., and Jensen K. J. 1973. Mineralogy, mineral-chemistry, and composition of the Murchison (C2) meteorite. *Smithsonian Contributions to the Earth Sciences* 10:1–38.

Gomes C. B. and Keil K. 1980. *Brazilian stone meteorites*. Albuquerque, New Mexico: University of New Mexico Press. 161 pp.

Graham A. L., Easton A. J., and Hutchison R. 1977. Forsterite chondrites; the meteorites Kakangari, Mount Morris (Wisconsin), Pontlyfni, and Winona. *Mineralogical Magazine* 41:201–210.

Greenwood R. C., Franchi I. A., Kearsley A. T., and Alard O. 2010. The relationship between CK and CV chondrites. *Geochimica et Cosmochimica Acta* 74:1684–1705.

Grossman J. N. and Brearley A. J. 2005. The onset of metamorphism in ordinary and carbonaceous chondrites. *Meteoritics & Planetary Science* 40:87–122.

Grossman J. N., Rubin A. E., Rambaldi E. R., Rajan R. S., and Wasson J. T. 1985. Chondrules in the Qingzhen type-3 enstatite chondrite: Possible precursor components and comparison to ordinary chondrite chondrules. *Geochimica et Cosmochimica Acta* 49:1781–1795.

Grossman J. N., Rubin A. E., Nagahara H., and King E. A. 1988. Properties of chondrules. In *Meteorites and the early solar system*, edited by Kerridge J. F. and Matthews M. S. Tucson, Arizona: The University of Arizona Press. pp. 619–659.

Grossman L., Allen J. M., and MacPherson G. J. 1980. Electron microprobe study of a "mysterite"-bearing inclusion from the Krymka LL-chondrite. *Geochimica et Cosmochimica Acta* 44:211–216.

Hewins R. H., Bourot-Denise M., Zanda B., Leroux H., Barrat J.-A., Humayun M., Göpel C., Greenwood R. C., Franchi I. A., Pont S., Lorand J.-P., Cournède C., Gattacceca J., Rochette P., Kuga M., Marrocchi Y., and Marty B. 2014. The Paris meteorite, the least altered CM chondrite so far. *Geochimica et Cosmochimica Acta* 124:190–222.

Hurt S. M., Rubin A. E., and Wasson J. T. 2012. Fractionated matrix composition in CV3 Vigarano and alteration processes on the CV parent asteroid. *Meteoritics & Planetary Science* 47:1035–1048.

Huss G. R., Keil K., and Taylor G. J. 1981. The matrices of unequilibrated ordinary chondrites: Implications for the origin and history of chondrites. *Geochimica et Cosmochimica Acta* 45:33–51.

Huss G. R., Rubin A. E., and Grossman J. N. 2006. Thermal metamorphism in chondrites. In *Meteorites and the early solar system II*, edited by Lauretta D., Leshin L. A., and McSween H. Y. Tucson, Arizona: The University of Arizona Press. pp. 567–586.

Hutchison R. 2004. *Meteorites: A petrologic, chemical and isotopic synthesis*. Cambridge: Cambridge University Press. 506 pp.

Ikeda Y., Kimura M., Mori H., and Takeda H. 1981. Chemical compositions of matrices of unequilibrated ordinary chondrites. *Memoirs of the National Institute of Polar Research (Japan), Special Issue* 17:124–144.

Jarosewich E. 1990. Chemical analyses of meteorites: A compilation of stony and iron meteorite analyses. *Meteoritics* 25:323–337.

Johnson J. M., Zolensky M. E., Chan Q., and Kring D. A. 2015. Striking graphite-bearing clasts found in two ordinary chondrite samples: NWA 6169 & NWA 8330. Northeast Regional GSA 2015 Abstracts with Program.

Kallemeyn G. W. and Rubin A. E. 1995. Coolidge and Loongana 001: A new carbonaceous chondrite grouplet. *Meteoritics* 30:20–27.

Kallemeyn G. W., Rubin A. E., and Wasson J. T. 1994. The compositional classification of chondrites: VI. The CR carbonaceous chondrite group. *Geochimica et Cosmochimica Acta* 58:2873–2888.

Kallemeyn G. W., Rubin A. E., and Wasson J. T. 1996. The compositional classification of chondrites VII. The R chondrite group. *Geochimica et Cosmochimica Acta* 60:2243–2256.

Keil K. 1968. Mineralogical and chemical relationships among enstatite chondrites. *Journal of Geophysical Research* 73:6945–6976.

Keil K. and Fodor R. V. 1980. Origin and history of the polymict-brecciated Tysnes Island chondrite and its carbonaceous and non-carbonaceous lithic fragments. *Chemie der Erde* 39:1–26.

Kimura M., Barrat J. A., Weisberg M. K., Imae N., Yamaguchi A., and Kojima H. 2014. Petrology and bulk chemistry of Yamato-82094, a new type of carbonaceous chondrite. *Meteoritics & Planetary Science* 49:346–357.

Kita N. T., Nagahara H., Tachibana S., Tomomura S., Spicuzza M. J., Fournelle J. H., and Valley J. W. 2010. High precision SIMS oxygen three isotope study of chondrules in LL3 chondrites: Role of ambient gas during chondrule formation. *Geochimica et Cosmochimica Acta* 74:6610–6635.

Kita N. T., Tenner T. J., Ushikubo T., Nakashima D., and Bischoff A. 2013. Primitive chondrules in a highly unequilibrated clast in NWA 753 R chondrite (abstract #1784). 44th Lunar and Planetary Science Conference. CD-ROM.

Kita N. T., Tenner T. J., Defouilloy C., Nakashima D., Ushikubo T., and Bischoff A. 2015. Oxygen isotope systematics of chondrules in R3 clasts: A genetic link to ordinary chondrites (abstract #2053). 46th Lunar and Planetary Science Conference. CD-ROM.

Krot A. N., Keil K., Goodrich C. A., and Scott E. R. D. 2005. Classification of meteorites. In *Meteorites, comets, and planets*, edited by Davis A. M. Amsterdam: Elsevier. pp. 83–128.

Kurat G. 1970. Zur Genese des kohligen Materials im Meteoriten von Tieschitz. *Earth and Planetary Science Letters* 7:317–324.

Leitch C. A. and Grossman L. 1977. Lithic clasts in the Supuhee chondrite. *Meteoritics* 12:125–139.

Lipschutz M. E., Gaffey M. J., and Pellas P. 1989. Meteoritic parent bodies: Nature, number, size and relation to present-day asteroids. In *Asteroids III*, edited by Bottke W. F., Cellino A., Paolicchi P. and Binzel R. P. Tucson, Arizona: The University of Arizona Press. pp. 740–777.

MacPherson G. J. 2005. Calcium-aluminum-rich inclusions in chondritic meteorites. In *Meteorites, comets, and planets*, edited by Davis A. M. Treatise on Geochemistry, vol. 1. Amsterdam: Elsevier. pp. 201–246.

Marrocchi Y., Gounelle M., Blanchard I., Caste F., and Kearsley A. T. 2014. The Paris CM chondrite: Secondary minerals and asteroidal processing. *Meteoritics & Planetary Science* 49:1232–1249.

Mason B. 1966. The enstatite chondrites. *Geochimica et Cosmochimica Acta* 30:23–39.

Mason B. and Wiik H. B. 1962. The Renazzo meteorite. *American Museum Novitates* 2106:1–11.

McSween H. Y. 1977a. Carbonaceous chondrites of the Ornans type: A metamorphic sequence. *Geochimica et Cosmochimica Acta* 41:477–491.

McSween H. Y. 1977b. Petrographic variations among carbonaceous chondrites of the Vigarano type. *Geochimica et Cosmochimica Acta* 41:1777–1790.

McSween H. Y. 1979. Alteration in CM carbonaceous chondrites inferred from modal and chemical variations in matrix. *Geochimica et Cosmochimica Acta* 43:1761–1770.

McSween H. Y. and Richardson S. M. 1977. The composition of carbonaceous chondrite matrix. *Geochimica et Cosmochimica Acta* 41:1145–1161.

Nagahara H. 1984. Matrices of type 3 ordinary chondrites—Primitive nebular records. *Geochimica et Cosmochimica Acta* 48:2581–2595.

Nakagawa Y., Sekiya M., and Hayashi C. 1986. Settling and growth of dust particles in a laminar phase of a low mass solar nebula. *Icarus* 67:375–390.

Nakamura-Messenger K., Clemett S. J., Rubin A. E., Choi B.-G., Zhang S., Rahman Z., Oikawa K., and Keller L. P. 2012. Wassonite: A new titanium monosulfide mineral in the Yamato 691 enstatite chondrite. *American Mineralogist* 97:807–815.

Nelson V. E. and Rubin A. E. 2002. Size-frequency distributions of chondrules and chondrule fragments in LL3 chondrites: Implications for parent-body fragmentation of chondrules. *Meteoritics & Planetary Science* 37:1361–1376.

Newton J., Bischoff A., Arden J. W., Franchi I. A., Geiger T., Greshake A., and Pillinger C. T. 1995. Acfer 094, a uniquely primitive carbonaceous chondrite from the Sahara. *Meteoritics* 30:47–56.

Nozette S. and Wilkening L. L. 1982. Evidence for aqueous alteration in a carbonaceous xenolith from the Plainview (H5) chondrite. *Geochimica et Cosmochimica Acta* 46:557–563.

Olsen E. and Jarosewich E. 1971. Chondrules: First occurrence in an iron meteorite. *Science* 174:583–585.

Rubin A. E. 1982. *Petrology and origin of brecciated chondritic meteorites*. Ph.D. dissertation, University of New Mexico, Albuquerque. 220 pp.

Rubin A. E. 1984. Coarse-grained chondrule rims in type 3 chondrites. *Geochimica et Cosmochimica Acta* 48:1779–1789.

Rubin A. E. 1989. An olivine-microchondrule-bearing clast in the Krymka meteorite. *Meteoritics* 24:191–192.

Rubin A. E. 1990. Kamacite and olivine in ordinary chondrites: Intergroup and intragroup relationships. *Geochimica et Cosmochimica Acta* 54:1217–1232.

Rubin A. E. 1992. A shock-metamorphic model for silicate darkening and compositionally variable plagioclase in CK and ordinary chondrites. *Geochimica et Cosmochimica Acta* 56:1705–1714.

Rubin A. E. 1997. Sinoite (Si_2N_2O): Crystallization from EL chondrite impact melts. *American Mineralogist* 82:1001–1006.

Rubin A. E. 2000. Petrologic, geochemical and experimental constraints on models of chondrule formation. *Earth-Science Reviews* 50:3–27.

Rubin A. E. 2005. Relationships among intrinsic properties of ordinary chondrites: Oxidation state, bulk chemistry, oxygen-isotopic composition, petrologic type and chondrule size. *Geochimica et Cosmochimica Acta* 69:4907–4918.

Rubin A. E. 2007. Petrography of refractory inclusions in CM2.6 QUE 97990 and the origin of melilite-free spinel inclusions in CM chondrites. *Meteoritics & Planetary Science* 42:1711–1726.

Rubin A. E. 2010. Physical properties of chondrules in different chondrite groups: Implications for multiple melting events in dusty environments. *Geochimica et Cosmochimica Acta* 74:4807–4828.

Rubin A. E. 2011. Origin of the differences in refractory-lithophile-element abundances among chondrite groups. *Icarus* 213:547–558.

Rubin A. E. 2014. Shock and annealing in the amphibole- and mica-bearing R chondrites. *Meteoritics & Planetary Science* 49:1057–1075.

Rubin A. E. 2015. An American on Paris: Extent of aqueous alteration of a CM chondrite and the petrography of its refractory and amoeboid olivine inclusions. *Meteoritics & Planetary Science* 50:1595–1612.

Rubin A. E. and Bottke W. F. 2009. On the origin of shocked and unshocked CM clasts in H-chondrite regolith breccias. *Meteoritics & Planetary Science* 44:701–724.

Rubin A. E. and Grossman J. N. 1987. Size-frequency-distributions of EH3 chondrules. *Meteoritics* 22:237–251.

Rubin A. E. and Kallemeyn G. W. 1989. Carlisle Lakes and Allan Hills 85151: Members of a new chondrite grouplet. *Geochimica et Cosmochimica Acta* 53:3035–3044.

Rubin A. E. and Kallemeyn G. W. 1993. Carlisle Lakes chondrites: Relationship to other chondrite groups (abstract). *Meteoritics* 28:424–425.

Rubin A. E. and Kallemeyn G. W. 1994. Pecora Escarpment 91002: A member of the new Rumuruti (R) chondrite group. *Meteoritics* 29:255–264.

Rubin A. E., Scott E. R. D., Taylor G. J., Keil K., Allen J. S. B., Mayeda T. K., Clayton R. N., and Bogard D. D. 1983. Nature of the H chondrite parent body regolith: Evidence from the Dimmitt breccia. Proceedings, 13th Lunar and Planetary Science Conference. pp. A741–A754.

Rubin A. E., James J. A., Keck B. D., Weeks K. S., Sears D. W. G., and Jarosewich E. 1985. The Colony meteorite and variations in CO3 chondrite properties. *Meteoritics* 20:175–196.

Rubin A. E., Trigo-Rodríguez J. M., Kunihiro T., Kallemeyn G. W., and Wasson J. T. 2005. Carbon-rich chondritic clast PV1 from the Plainview H-chondrite regolith breccia: Formation from H3 chondrite material by possible cometary impact. *Geochimica et Cosmochimica Acta* 69:3419–3430.

Rubin A. E., Trigo-Rodríguez J. M., Huber H., and Wasson J. T. 2007. Progressive aqueous alteration of CM carbonaceous chondrites. *Geochimica et Cosmochimica Acta* 71:2361–2382.

Rubin A. E., Griset C. D., Choi B.-G., and Wasson J. T. 2009. Clastic matrix in EH3 chondrites. *Meteoritics & Planetary Science* 44:589–601.

Scott E. R. D. and Taylor G. J. 1982. Primitive breccias among type 3 ordinary chondrites–Origin and relation to regolith breccias. In *Workshop on lunar breccias and soils and their meteoritic analogs*, edited by Taylor G. J. and Wilkening L. L. LPI Technical Report 82-02. Houston, Texas: Lunar and Planetary Institute. pp. 130–134.

Scott E. R. D., Taylor G. J., Rubin A. E., Okada A., and Keil K. 1981. Graphite-magnetite aggregates in ordinary chondritic meteorites. *Nature* 291:544–546.

Scott E. R. D., Rubin A. E., Taylor G. J., and Keil K. 1984. Matrix material in type 3 chondrites—Occurrence,

heterogeneity and relationship with chondrules. *Geochimica et Cosmochimica Acta* 48:1741–1757.

Scott E. R. D., Brearley A. J., Keil K., Grady M. M., Pillinger C. T., Clayton R. N., Mayeda T. K., Wieler R., and Signer P. 1988. Nature and origin of C-rich ordinary chondrites and chondritic clasts. Proceedings, 18th Lunar and Planetary Science Conference. pp. 513–523.

Semenenko V. P. and Perron C. 2005. Shock-melted material in the Krymka LL3.1 chondrite: Behavior of the opaque minerals. *Meteoritics & Planetary Science* 40:173–185.

Semenenko V. P., Jessberger E. K., Chaussidon M., Weber I., Stephan T., and Wies C. 2005. Carbonaceous xenoliths in the Krymka LL3.1 chondrite: Mysteries and established facts. *Geochimica et Cosmochimica Acta* 69:2165–2182.

Stöffler D., Keil K., and Scott E. R. D. 1991. Shock metamorphism of ordinary chondrites. *Geochimica et Cosmochimica Acta* 55:3845–3867.

Takagi M. 2005. Compositional distributions of olivine and low-Ca pyroxene in chondrules from LL3.0 Semarkona: Development of a numerical computer model to simulate the olivine distribution and implications for chondrule formation. M.S. thesis, University of California at Los Angeles, Los Angeles, California. 149 p.

Tomeoka K., Kojima T., Ohnishi I., Ishii Y., and Nakamura N. 2005. The Kobe CK carbonaceous chondrite: Petrography, mineralogy and metamorphism. *Journal of Mineralogical and Petrological Sciences* 100:116–125.

Van Roosbroek N., Debaille V., Pittarello L., Goderis S., Humayun M., Hecht L., Jourdan F., Spicuzza M. J., Vanhaecke F., and Claeys P. 2015. The formation of IIE iron meteorites investigated by the chondrule-bearing Mont Dieu meteorite. *Meteoritics & Planetary Science* 50:1173–1196.

Van Schmus W. R. 1969. Mineralogy, petrology, and classification of types 3 and 4 carbonaceous chondrites. In *Meteorite research*, edited by Millman P. M. Dordrecht, the Netherlands: D. Reidel Publishing Company. pp. 480–491.

Wasson J. T. 2008. Evaporation of nebular fines during chondrule formation. *Icarus* 195:895–907.

Wasson J. T., Isa J., and Rubin A. E. 2013. Compositional and petrographic similarities of CV and CK chondrites: A single group with variations in textures and volatiles attributable to impact heating, crushing and oxidation. *Geochimica et Cosmochimica Acta* 108:45–62.

Weidenschilling S. J. 1977. Aerodynamics of solid bodies in the solar nebula. *Monthly Notices of the Royal Astronomical Society* 180:57–70.

Weisberg M. K. and Kimura M. 2012. The unequilibrated enstatite chondrites. *Chemie der Erde* 72:101–115.

Weisberg M. K. and Prinz M. 1994. Agglomeratic olivine (AO) chondrules in ordinary chondrites (abstract). 25th Lunar and Planetary Science Conference.p. 1481.

Weisberg M. K. and Prinz M. 1996. Agglomeratic chondrules, chondrule precursors, and incomplete melting. In *Chondrules and the protoplanetary disk*, edited by Hewins R. H., Jones R. H., and Scott E. R. D.. Cambridge: Cambridge University Press. pp. 119–127.

Weisberg M. K., Prinz M., Clayton R. N., and Mayeda T. K. 1993. The CR (Renazzo-type) carbonaceous chondrite group and its implications. *Geochimica et Cosmochimica Acta* 57:1567–1586.

Weisberg M. K., Prinz M., Clayton R. N., Mayeda T. K., Grady M. M., Franchi I., Pillinger C. T., and Kallemeyn G. W. 1996. The K (Kakangari) chondrite grouplet. *Geochimica et Cosmochimica Acta* 60:4253–4263.

Weisberg M. K., Ebel D. S., Connolly H. C., Kita N. T., and Ushikubo T. 2011. Petrology and oxygen isotope compositions of chondrules in E3 chondrites. *Geochimica et Cosmochimica Acta* 75:6556–6569.

Williams C. V., Rubin A. E., Keil K., and San Miguel A. 1985. Petrology of the Cangas de Onis and Nulles regolith breccias: Implications for parent body history. *Meteoritics* 20:331–345.

Wlotzka F. 1993. A weathering scale for the ordinary chondrites (abstract). *Meteoritics* 28:460.

Wood J. A. 1967. Olivine and pyroxene compositions in Type II carbonaceous chondrites. *Geochimica et Cosmochimica Acta* 31:2095–2108.

Young E. D., Yeung L. Y., and Kohl I. E. 2014. On the $\Delta^{17}O$ budget of atmospheric O_2. *Geochmica eet Cosmochimica Acta* 135:102–125.

Zolensky M. and Ivanov A. 2003. The Kaidun microbreccia meteorite: A harvest from the inner and outer asteroid belt. *Chemie der Erde* 63:185–246.

Zolensky M., Barrett R., and Browning L. 1993. Mineralogy and composition of matrix and chondrule rims in carbonaceous chondrites. *Geochimica et Cosmochimica Acta* 57:3123–3148.

Zolensky M. E., Weisberg M. K., Buchanan P. C., and Mittlefehldt D. W. 1996. Mineralogy of carbonaceous chondrite clasts in HED achondrites and the Moon. *Meteoritics & Planetary Science* 31:518–537.

Zolensky M. E., Clayton R. N., Mayeda T., Chokai J., and Norton O. R. 2003. Carbonaceous chondrite clasts in the halite-bearing H5 chondrite Zag (abstract). *Meteoritics & Planetary Science* 38:A114.

Zolensky M. E., Fries M., Chan Q. H.-S., Kebukawa Y., Steele A., and Bodnar R. J. 2015. The mineralogy of Ceres* (*or something an awful lot like it) (abstract #5270). 78th Annual Meeting of the Meteoritical Society.